Wavelet-Based Fault Detection of a Single-Phase Transformerless Grid-Connected Photovoltaic Inverter System

Orogun O, Emmanuel[1], Akinseloyin G, Aarinola[2], Ogundipe R, Josiah[3]

Department of Electrical & Electronics Engineering, Faculty of Engineering, Federal University, Oye-Ekiti, Nigeria

DOI: https://doi.org/10.51584/IJRIAS.2026.11030093

Received: 26 March 2026; Accepted: 31 March 2026; Published: 15 April 2026

ABSTRACT

The increasing global transition towards renewable energy has highlighted the critical role of photovoltaic (PV) systems in sustainable electricity generation. This research investigates fault detection techniques for single-phase transformerless grid-connected PV systems using advanced wavelet-based analysis and machine learning classifiers. Focusing on critical system components, the study explores fault scenarios including DC link capacitor, IGBT, ground fault, AC filter capacitor, and short circuit conditions. By implementing Discrete Wavelet Transform (DWT) with Daubechies-4 mother wavelet and extracting statistical features, the research developed a comprehensive fault detection framework. Three machine learning models Support Vector Classification, Random Forest, and Neural Network were evaluated for fault classification accuracy. Results of the research reveals that the neural network model achieved the highest overall accuracy at 99.46%, followed by Random Forest at 99.40%, and Support Vector Classification at 99.20%. The precision metrics indicate superior performance of the SVC model in correctly identifying positive cases across all fault categories. The recall values demonstrate the models' effectiveness in identifying all relevant instances of each fault type, with the neural network model showing strength in this aspect. The results demonstrated exceptional performance, highlighting the potential of wavelet-based techniques in enhancing PV system reliability and safety. The methodology provides a robust approach for near real-time capable fault detection in simulation environments, offering significant implications for improving renewable energy infrastructure resilience.

INTRODUCTION

The global energy sector has transformed significantly in recent decades, driven by the urgent need to reduce greenhouse gas emissions and address climate change (Bahman, 2023; Gielen & Boshell, 2019). Renewable energy sources, particularly photovoltaic (PV) systems, have become critical alternatives to fossil fuels due to their sustainability, decreasing costs, and adaptability (Shahsavari & Akbari, 2018; Jaiswal et al., 2022). PV systems convert sunlight into electricity through the photovoltaic effect and are broadly categorised into grid-connected and stand-alone configurations. Stand-alone systems are typically used in remote or off-grid areas, while grid-connected systems integrate with existing electrical grids, enabling energy exchange and enhancing infrastructure resilience (Maka & Alabid, 2022; Shahsavari & Akbari, 2018).

Grid-connected PV systems have expanded rapidly, supported by policy incentives, technological advancements, and environmental awareness (Panagode et al., 2023). These systems reduce transmission losses, improve energy efficiency, and support load balancing by generating electricity near consumption points (Guo et al., 2024). However, traditional grid-connected systems often use transformers for electrical isolation, increasing costs, weight, and energy losses (Sudipto et al., 2024). Transformerless configurations have emerged as a cost-effective alternative, eliminating transformers to improve efficiency and reduce installation expenses (Ali et al., 2022). Despite these benefits, the absence of galvanic isolation raises safety concerns, such as leakage currents and electromagnetic interference, which require careful management (Madasamy et al., 2019).

Reliable fault detection is essential for the safe operation of transformerless systems. Conventional methods often rely on complex models or costly hardware, limiting their practicality (Suganya et al., 2023). Wavelet-

based techniques offer a promising solution, enabling precise analysis of transient signals to detect faults like ground faults or insulation failures (Abdelelah et al., 2022). This approach decomposes signals into time-frequency components, identifying anomalies even in noisy environments (Murugesan & Sathish, 2021).

This study investigates the application of wavelet-based fault detection in single-phase transformerless grid-connected PV systems through simulation. By developing and validating a robust model and algorithm, the research aims to enhance system reliability and safety, supporting wider adoption of this sustainable technology (Xiaotong et al., 2022; Yao et al., 2020). Successful implementation could improve efficiency and resilience, contributing to global renewable energy goals.

Empirical Review and Research Gap

The field of single-phase transformerless grid-connected photovoltaic (PV) systems has seen significant advancements in recent years, particularly in the areas of system design, control strategies, and fault detection techniques. This review synthesises key findings from relevant studies, focusing on their contributions to fault detection and system performance improvement.

Arafa et al. (2017) and Raghuwanshi and Gupta (2015) conducted comprehensive studies on single-phase grid-connected PV systems using different approaches. Arafa et al. examined a single-stage system using MATLAB/Simulink simulations and experimental validation with a MicrolabBox DSP prototyping platform, whilst Raghuwanshi and Gupta simulated a double-stage system with carefully designed controllers. Both studies emphasised the importance of maximum power point tracking (MPPT), voltage control, and current control.

Liu et al. (2020) advanced these earlier works by proposing a novel topology for single-phase transformerless PV inverters that significantly reduced leakage current whilst maintaining high efficiency. Their design incorporated a switched-capacitor circuit, enabling better utilisation of the DC link voltage and improved power quality. Simulation and experimental results demonstrated the effectiveness of this approach in reducing electromagnetic interference and improving overall system performance.

Afshari et al. (2015) and Boonmee and Kumsuwan (2015) explored different aspects of inverter design and control. Afshari et al. analysed a full-bridge inverter with a DC bypass, highlighting its efficiency and ability to minimise leakage current. Boonmee and Kumsuwan focused on implementing advanced control techniques, specifically the ripple correlation control for MPPT and current control in a rotating reference frame.

Zhang et al. (2021) built upon these control strategies by introducing an adaptive backstepping control method for single-phase grid-connected PV inverters. Their approach demonstrated superior performance in terms of faster dynamic response and better disturbance rejection compared to traditional PI controllers. The adaptive nature of their controller allowed it to maintain optimal performance even under varying grid conditions and system parameter uncertainties.

Recent research has made significant strides in fault detection and protection strategies for grid-connected PV systems. Khan et al. (2022) and Ahmad et al. (2018) employed machine learning techniques for fault detection using different approaches. Khan et al. used wavelet transform for signal processing and a support vector data descriptor (SVDD) as a classifier, achieving high accuracy and fast detection times for various islanding conditions. Ahmad et al. developed a more comprehensive algorithm using wavelet transform and neural networks to detect a wider range of faults, including partial shading and component failures.

Liao et al. (2023) advanced the field further by proposing a novel fault diagnosis method based on a hybrid deep learning model. Their approach combined convolutional neural networks (CNNs) for feature extraction with long short-term memory (LSTM) networks for temporal dependency modelling. This hybrid model demonstrated superior accuracy in detecting and classifying various faults in single-phase PV systems, including inverter faults, PV array faults, and grid anomalies.

Chen et al. (2022) introduced a real-time fault detection and classification system using edge computing and federated learning. Their approach enabled distributed fault detection across multiple PV installations whilst preserving data privacy. The system showed impressive performance in detecting incipient faults, potentially reducing maintenance costs and improving overall system reliability.

Benabdelkader et al. (2023) and Perpinias et al. (2015) addressed different aspects of grid integration and power quality. Benabdelkader et al. proposed a control method to improve power quality at the point of common coupling (PCC), demonstrating enhanced performance and robustness against grid fluctuations. Perpinias et al. focused on meeting Fault Ride Through requirements, proposing a control paradigm that enables PV systems to assist during faults by injecting reactive power.

Wang et al. (2024) expanded on these concepts by developing an advanced grid-supportive control strategy for single-phase PV inverters. Their method allowed PV systems to provide ancillary services to the grid, including voltage regulation and frequency support, without compromising their primary power generation function. Simulation results showed that this approach could significantly enhance grid stability in areas with high PV penetration.

Kibria et al. (2023) and Barkat et al. (2023) provided comprehensive comparative analyses offering valuable insights for future research directions. Kibria et al. simulated and compared 18 different inverter topologies, analysing their common-mode characteristics and power loss distribution. Barkat et al. focused on comparing active islanding detection methods, including Active Frequency Drift (AFD), Sandia Frequency Shift (SFS), Slip Mode Frequency Shift (SMS), and Sandia Voltage Shift (SVS).

Rodriguez et al. (2024) built on these comparative studies by conducting an extensive review of fault detection techniques in single-phase PV systems, covering methods from traditional model-based approaches to advanced AI-driven techniques. Their analysis provided a comprehensive framework for selecting appropriate fault detection methods based on system characteristics and performance requirements.

A critical analysis of existing literature reveals significant research gaps in fault detection approaches for single-phase transformerless grid-connected PV systems. Whilst Khan et al. (2022) and Ahmad et al. (2018) implemented machine learning techniques for fault detection, their work primarily focused on specific fault scenarios, particularly islanding conditions and partial shading, without addressing the comprehensive range of component-level faults that commonly occur in transformerless PV systems. Furthermore, the research conducted by Chen et al. (2022) and Wang et al. (2024) predominantly concentrated on grid integration aspects and control strategies, with limited attention to the systematic analysis of multiple fault scenarios, particularly DC link capacitor and IGBT faults in transformerless topologies. Additionally, whilst Rodriguez et al. (2024) provided an extensive review of fault detection techniques, there remains a notable gap in comparative analysis of different machine learning classifiers' performance specifically for wavelet-based feature extraction in transformerless PV systems. While previous studies have demonstrated the effectiveness of wavelet transforms and machine learning in PV fault detection, their methodological choices often focus on single classifier approaches or limited fault scenarios. This study builds upon these works by integrating multi-resolution wavelet feature extraction with a comparative evaluation of three classifiers (SVC, RF, NN). Unlike Khan et al. (2022) and Ahmad et al. (2018), which focus on specific fault types, this research adopts a multi-fault framework, thereby improving generalisation and robustness of the detection system

RESEARCH METHODOLOGY

Research Design

This research employs a systematic approach to developing and simulating a wavelet-based fault detection system for single-phase transformerless grid-connected PV systems. As illustrated in Figure 1, the research design comprises several interconnected stages that collectively form a comprehensive framework for system modelling and analysis.

ISSN No. 2454-6194 | DOI: 10.51584/IJRIAS |Volume XI Issue III March 2026

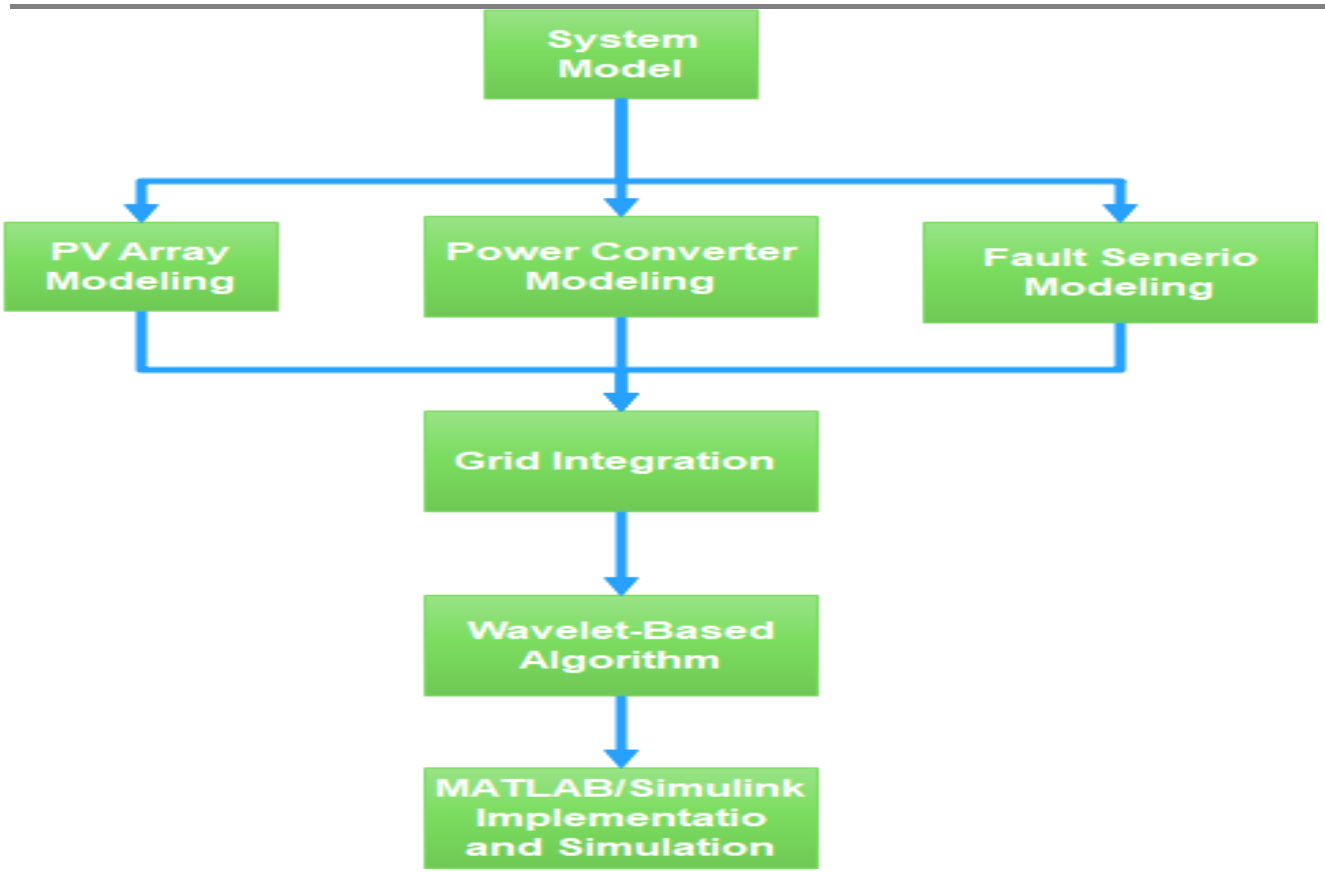

Figure 1**:** Methodology Flow Diagram

The system model, which forms the cornerstone of this research, is divided into three parallel development tracks: PV Array Modelling, Power Converter Modelling, and Fault Scenario Modelling. These three components are developed concurrently to ensure their seamless integration and interaction within the overall system architecture. The PV Array Modelling focuses on accurately representing the photovoltaic generation characteristics, whilst the Power Converter Modelling encompasses the transformerless inverter topology and its associated control systems. The Fault Scenario Modelling introduces various fault conditions that commonly occur in transformerless PV systems.

These three modelling components converge at the Grid Integration stage, where their interactions are analysed and optimised to ensure proper system operation under both normal and fault conditions. This integration phase is crucial for validating the system's behaviour and performance when connected to the utility grid.

Following the grid integration, the research implements a Wavelet-Based Algorithm for fault detection and classification. This algorithm processes the system's electrical signals to extract relevant features that can indicate the presence and nature of various faults.

The final stage involves the implementation and simulation of the complete system using MATLAB/Simulink. This platform provides the necessary tools and flexibility to validate the proposed fault detection approach through comprehensive simulations under various operating conditions and fault scenarios.

This structured research design ensures a methodical investigation of the wavelet-based fault detection system, allowing for thorough validation of its effectiveness in identifying and classifying faults in transformerless grid-connected PV systems.

Solar PV Model

The photovoltaic array model employed in this research utilises the Canadian Solar Inc. CS3U-375MS-AG module configuration, implemented through MATLAB/Simulink's PV Array block. The system comprises 2

ISSN No. 2454-6194 | DOI: 10.51584/IJRIAS |Volume XI Issue III March 2026

parallel strings, each containing 10 series-connected modules, yielding a total system capacity of 7.5 kW under standard test conditions (STC).

The mathematical model of the PV cell is based on the single-diode equivalent circuit shown in Figure 2, which can be expressed through the following equations. The output current (I) of the PV cell is given by Equation 1 (Hossain *et al*. 2016):

$$I = I_{ph} - I_d - I_{sh} \qquad (1)$$

where I_{ph} represents the photogenerated current, I_d is the diode current, and I_sh is the current through the shunt resistance. The diode current I_d follows the Shockley diode equation as shown in Equation 2:

$$I_d = I_0 \left[\exp\left(\frac{V + IR_s}{nV_t}\right) - 1\right] \qquad (2)$$

where I_0 is the diode saturation current $(2.473 \times 10^{-11} A)$, V is the cell voltage, R_s is the series resistance (0.24088 Ω), n is the diode ideality factor (0.96345), and V_t is the thermal voltage given by:

$$V_t = \frac{kT}{q} \qquad (3)$$

where k is Boltzmann's constant, T is the cell temperature in Kelvin, and q is the electron charge.

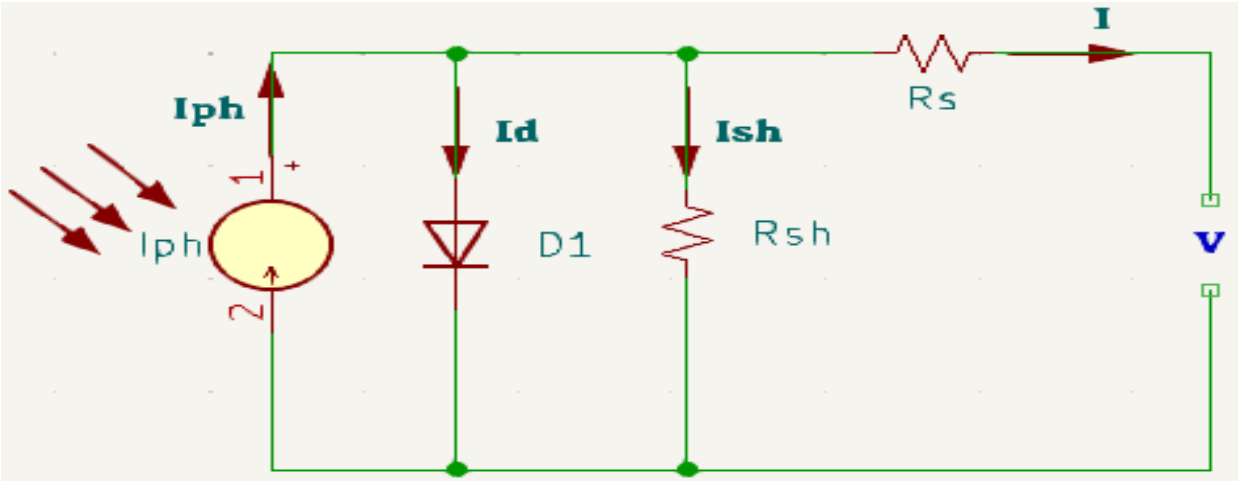

Figure 2: Equivalent Circuit of Single-Diode PV Model (Shekhar, 2018)

The shunt current I_{sh} is calculated using Equation 4:

I_sh = (V + IR_s)/R_sh (4)

where R_sh is the shunt resistance (294.0017 Ω).

Table 1: PV Module Specifications and Parameters

Parameter	Value	Unit
Maximum Power (P_{max}	375.314	W
Open Circuit Voltage (V_{oc})	47.6	V
Short Circuit Current (I_{sc})	9.93	A
Voltage at Maximum Power (V_{mp})	39.8	V
Current at Maximum Power (I_{mp})	9.43	A
Number of Cells per Module	72	-
Temperature Coefficient of V_{oc}	-0.293	%/°C

Temperature Coefficient of I_{sc}	0.035005	%/°C

The array configuration accounts for temperature effects on both voltage and current, as indicated by the temperature coefficients listed in Table 1. The model accepts solar irradiance (W/m²) and cell temperature (°C) as input parameters, enabling simulation under various environmental conditions. The system is designed to operate optimally at an irradiance of 1000 W/m² and cell temperature of 25°C, with capability to simulate performance at lower irradiance levels of 500 W/m² and 100 W/m² for comprehensive analysis.

The light-generated current (I_{ph}) of 9.9881 A at standard test conditions forms the basis for the array's power generation capability, whilst the diode saturation current and ideality factor determine the array's voltage-current characteristics. The series and shunt resistances have been optimised to accurately represent real-world module behaviour, accounting for internal losses and leakage currents.

This detailed modelling approach ensures accurate representation of the PV array's electrical characteristics under various operating conditions, providing a robust foundation for subsequent fault detection analysis.

Inverter Model

The inverter topology implemented in this research consists of a DC coupling stage, a full-bridge converter, and an LC output filter. This configuration provides efficient power conversion whilst maintaining low harmonic distortion in the output waveform.

The DC coupling capacitor (C_{dc}) serves as an energy buffer between the PV array and the inverter. Its value is calculated using Equation 5:

$$C_{dc} = \frac{P_{rated}}{2\pi f_{grid} \times V_{dc} \times \Delta V_{dc}} \qquad (5)$$

where P_{rated} is 7.5 kW, f_grid is 50 Hz, V_{dc} is 400 V, and ΔV_{dc} is the allowable voltage ripple (2% of V_{dc}). This yields:

$$C_{dc} = \frac{7500}{2\pi \times 50 \times 400 \times 8} = 1490\ \mu F$$

The full-bridge converter employs four IGBTs with anti-parallel diodes, featuring an ON-state resistance ($R_{ds(on)}$) of $1\times10^{-3}\Omega$ and snubber resistance of $1\times10^{6}\ \Omega$. The converter operates with unipolar PWM switching at a frequency (f_{sw}) of 10 kHz to minimise switching losses whilst maintaining good power quality.

The LC low-pass filter parameters are determined based on the following design criteria. The filter inductance (L_f) is calculated using Equation 6:

$$L_f = \frac{V_{dc}}{4 \times f_{sw} \times \Delta I_L} \qquad (6)$$

where ΔI_L is the maximum allowable current ripple (20% of rated current). This results in:

$$L_f = \frac{400}{4 \times 10000 \times 6.8} = 1.47\ mH$$

The filter capacitance (C_f) is determined using Equation 7:

$$C_f = \frac{1}{(2\pi f_c)^2 \times L_f} \qquad (7)$$

where f_c is the cutoff frequency, typically set at one-tenth of the switching frequency. This gives:

ISSN No. 2454-6194 | DOI: 10.51584/IJRIAS |Volume XI Issue III March 2026

$$C_f = \frac{1}{(2\pi \times 1000)^2 \times 0.00147} = 17.2\ \mu F$$

Table 2: Inverter Parameters and Component Values

Parameter	Symbol	Value	Unit
Rated Power	P_{rated}	7500	W
DC Link Voltage	V_{dc}	400	V
Grid Voltage (RMS)	V_{grid}	230	V
Grid Frequency	f_{grid}	50	Hz
Switching Frequency	f_{sw}	10	kHz
DC Coupling Capacitor	C_{dc}	1500	µF
Filter Inductance	L_f	1.5	mH
Filter Capacitance	C_f	17	µF
IGBT On-state Resistance	$R_{ds(on)}$	1×10^{-3}	Ω
Snubber Resistance	R_{snub}	1×10^{6}	Ω
Damping Resistance	R_d	0.5	Ω

The values presented in Table 2 have been slightly adjusted from the calculated values to align with standard component values whilst maintaining optimal system performance. The damping resistance (R_d) is added in series with the filter capacitor to mitigate resonance effects at the filter's cutoff frequency.

This inverter configuration ensures efficient power conversion from the PV array to the grid whilst maintaining high power quality through effective filtering of switching harmonics. The component values have been carefully selected to balance system performance, efficiency, and practical implementation considerations.

Grid Model and Integration

The grid integration component of this research employs a simplified yet accurate representation of the utility grid using a single-phase AC voltage source. This model operates at the standard Nigeria grid parameters of 230V RMS at 50 Hz frequency, providing a stable reference for the inverter's grid-synchronisation system.

The grid model's impedance parameters are calculated based on typical short-circuit power levels at the point of common coupling (PCC). For a grid with short-circuit power (Ssc) of 1 MVA at 230V, the base impedance (Zbase) is determined using Equation 8:

$$Z_{base} = \frac{V_{grid}^2}{S_{sc}} \qquad (8)$$

This yields:

$$Z_{base} = \frac{230^2}{1 \times 10^6} = 0.0529$$

The grid inductance (Lg) and resistance (Rg) are then calculated assuming an X/R ratio of 10, which is typical for low-voltage distribution networks. The total grid impedance is typically 20% of the base impedance, distributed between inductive and resistive components according to Equations 9 and 10:

$$L_g = \frac{0.2 \times Z_{base} \times 10}{\sqrt{101} \times 2\pi f_{grid}} \qquad (9)$$

ISSN No. 2454-6194 | DOI: 10.51584/IJRIAS |Volume XI Issue III March 2026

$$R_g = \frac{0.2 \times Z_{base}}{\sqrt{101}} \qquad (10)$$

These calculations result in $Lg = 0.4\,mH\ and\ Rg = 0.1\,\Omega$.

The synchronisation mechanism employs a phase-locked loop (PLL) with parameters optimised for grid-connected operation. The PLL bandwidth (ωn) is selected based on the compromise between dynamic response and noise immunity, as shown in Equation 11:

$$\omega_n = \frac{2\pi}{20T_{grid}} \qquad (11)$$

where Tgrid is the grid period (20 ms), resulting in a natural frequency of 15.7 rad/s (2.5 Hz).

The complete grid model parameters are summarised in Table 3, presenting the calculated values and their associated operational limits for system integration.

Table 3: Grid Model Parameters and Operating Limits

Parameter	Symbol	Value
Nominal Voltage (RMS)	$Vgrid$	230 ± 10%V
Grid Frequency	$fgrid$	50 ± 0.5 Hz
Grid Inductance	Lg	0.4 mH
Grid Resistance	Rg	0.1 Ω
PLL Natural Frequency	ωn	15.7 rad/s
PLL Damping Ratio	ζ	0.707 -
Short Circuit Power	Ssc	1 MVA

This grid model framework enables comprehensive analysis of system behaviour under both normal operating conditions and fault scenarios. The parameters have been carefully selected and calculated to ensure realistic representation of grid characteristics whilst maintaining computational efficiency for subsequent fault analysis studies. The model's implementation in MATLAB/Simulink facilitates seamless integration with the PV array and inverter models described in previous sections, providing a robust platform for validating the proposed wavelet-based fault detection approach.

Fault Modelling

The fault scenarios investigated in this research focus on three critical system components: DC link capacitor, AC filter, and power circuit faults. These faults are selected based on their prevalence in transformerless grid-connected PV systems and their significant impact on system performance.

The DC link capacitor open circuit fault is modelled by introducing a series switch with the DC link capacitor (Cdc). Under normal operation, the switch remains closed, maintaining the capacitor's buffering function. During fault simulation, the switch opens, disconnecting the capacitor from the circuit. This fault condition significantly impacts the DC link voltage stability and can lead to increased voltage ripple, affecting power quality and system efficiency.

The mathematical representation of the DC link voltage behaviour under capacitor open circuit fault can be expressed through Equation 12:

$\frac{C_{dc}dV_{dc}}{dt} = I_{PV} - I_{inv}$	(12)

ISSN No. 2454-6194 | DOI: 10.51584/IJRIAS |Volume XI Issue III March 2026

During the open-circuit fault condition, the capacitor is effectively disconnected:

$$C_{dc} \rightarrow 0 \qquad (12.1)$$

$$\frac{dV_{dc}}{dt} = \frac{I_{PV} - I_{inv}}{C_{dc}} \qquad (12.2)$$

This represents an abrupt and uncontrolled variation in DC-link voltage, which is captured simulation through a controlled switch that isolates the capacitor

where i_{pv} is the PV array current and i_{inv} is the inverter input current. During the fault, Cdc effectively becomes zero, leading to theoretical infinite voltage variation.

The AC filter open circuit fault is implemented by introducing switching elements in series with the filter components (Lf and Cf). The fault condition is simulated by opening these switches, effectively removing the filtering capability. This fault affects the output current quality, as described by Equation 13:

$$i_{grid} = i_{inv} + \frac{d}{dt}(C_f v_{grid}) \qquad (13)$$

The short circuit fault scenario is modelled at the inverter output terminals through a controlled impedance path. The fault impedance (Zf) is set to 0.01 Ω to represent a low-impedance short circuit condition. The fault current (If) during this condition is governed by Equation 14:

$$I_f = \frac{V_{inv}}{Z_f} \qquad (14)$$

Impedance Path

The system response under these fault conditions is monitored through five key electrical parameters: AC voltage (Vac), AC current (Iac), DC voltage (Vdc), DC current (Idc), and leakage current (Ileakage). Data acquisition is performed at a sampling rate of 10 kHz to ensure adequate capture of transient behaviour. The collected data is exported to the MATLAB workspace for subsequent wavelet-based analysis using the Discrete Wavelet Transform (DWT) approach.

This comprehensive fault modelling approach enables systematic investigation of system behaviour under various fault conditions, providing the necessary data for developing and validating the proposed wavelet-based fault detection algorithm. The selection of fault scenarios and their implementation methods ensures realistic representation of common system failures while maintaining computational efficiency in the simulation environment.

Wavelet Analysis Model

The wavelet analysis model implemented in this research utilizes the Discrete Wavelet Transform (DWT) with Daubechies-4 (db4) mother wavelet for feature extraction, followed by multiple machine learning classifiers for fault detection and classification. The analysis framework processes five key electrical signals: AC voltage (Vac), AC current (Iac), DC voltage (Vdc), DC current (Idc), and leakage current (Ileakage).

The DWT decomposition is performed at level 4, providing both approximation and detail coefficients as shown in Figure 3. The wavelet decomposition process can be mathematically expressed through Equation 15:

$$x[n] = \sum_{k} c_{j_0,k}\, \phi_{j_0,k}[n] + \sum_{j=j_0}^{\infty} \sum_{k} d_{j,k}\, \psi_{j,k}[n] \qquad (15)$$

ISSN No. 2454-6194 | DOI: 10.51584/IJRIAS |Volume XI Issue III March 2026

where φ[n] represents the scaling function, ψ[n] is the wavelet function, $c_{j_0,k}$ are approximation coefficients at level j_0, and $d_{j,k}$ are detail coefficients at level j.

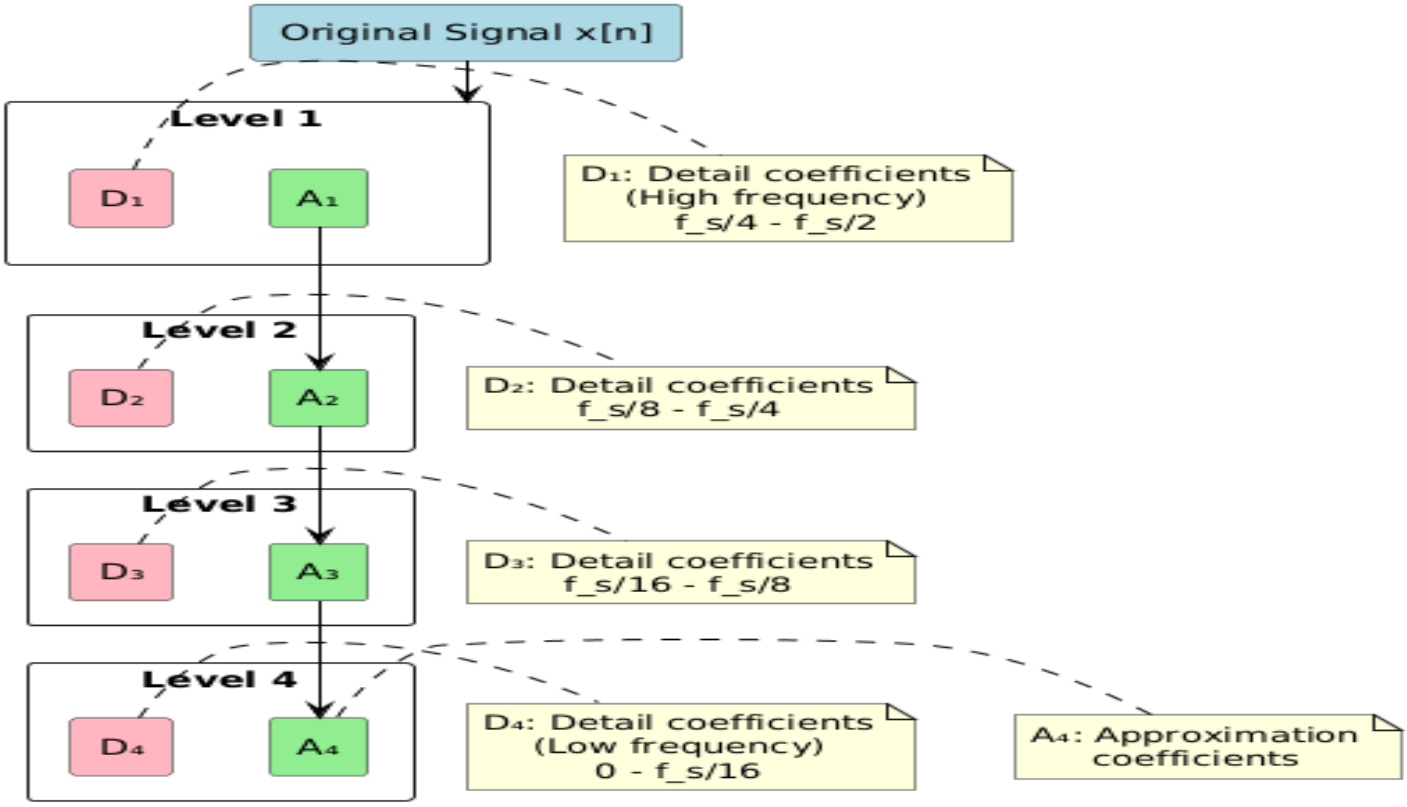

Figure 3: Wavelet Decomposition Structure

From each decomposition level, seven statistical features are extracted to form the feature vector. These features, calculated using Equations 16-22, include:

Mean Absolute Value: $MAV = \frac{1}{N}\sum_{i=1}^{N}|x_i|$ (16)

Standard Deviation: $\sigma = \sqrt{\frac{1}{N}\sum_{i=1}^{N}(x_i - \mu)^2}$ (17)

Skewness: $S = \frac{1}{N\sigma^3}\sum_{i=1}^{N}(x_i - \mu)^3$ (18)

Kurtosis: $K = \frac{1}{N\sigma^4}\sum_{i=1}^{N}(x_i - \mu)^4$ (19)

Root Mean Square: $RMS = \sqrt{\frac{1}{N}\sum_{i=1}^{N}x_i^2}$ (20)

Maximum Absolute Value: $MAV = max(|x_i|)$ (21)

Signal Energy: $E = \sum_{i=1}^{N}x_i^2$ (22)

The extracted features are normalized using z-score normalization before being fed into three different machine learning classifiers:

Support Vector Machine (SVM):

ISSN No. 2454-6194 | DOI: 10.51584/IJRIAS |Volume XI Issue III March 2026

The implemented SVM model uses a Radial Basis Function (RBF) kernel for multi-class classification as shown in Figure 4. The decision function is defined by Equation 23:

$$f(x) = sign\left(\sum_{i=1}^{N} \alpha_i\, y_i K(x_i, x) + b\right) \quad (23)$$

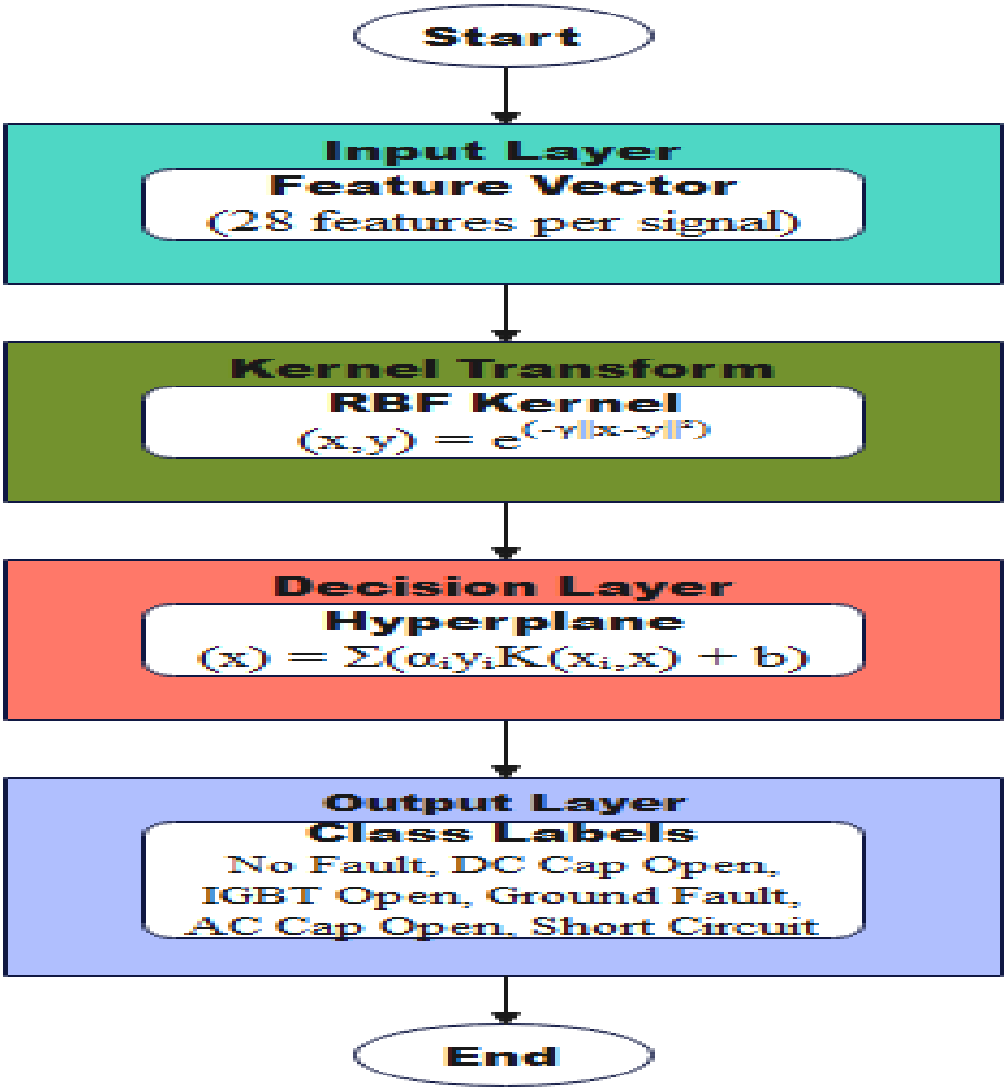

Figure 4: SVM Classification Model

Random Forest (RF):

An ensemble of 50 decision trees is implemented, with the final classification determined through majority voting. Each tree is constructed using the CART algorithm, with the split criterion defined by Equation 24:

$$Gini(t) = 1 - \sum_{i=1}^{c} p(i|t)^2 \quad (24)$$

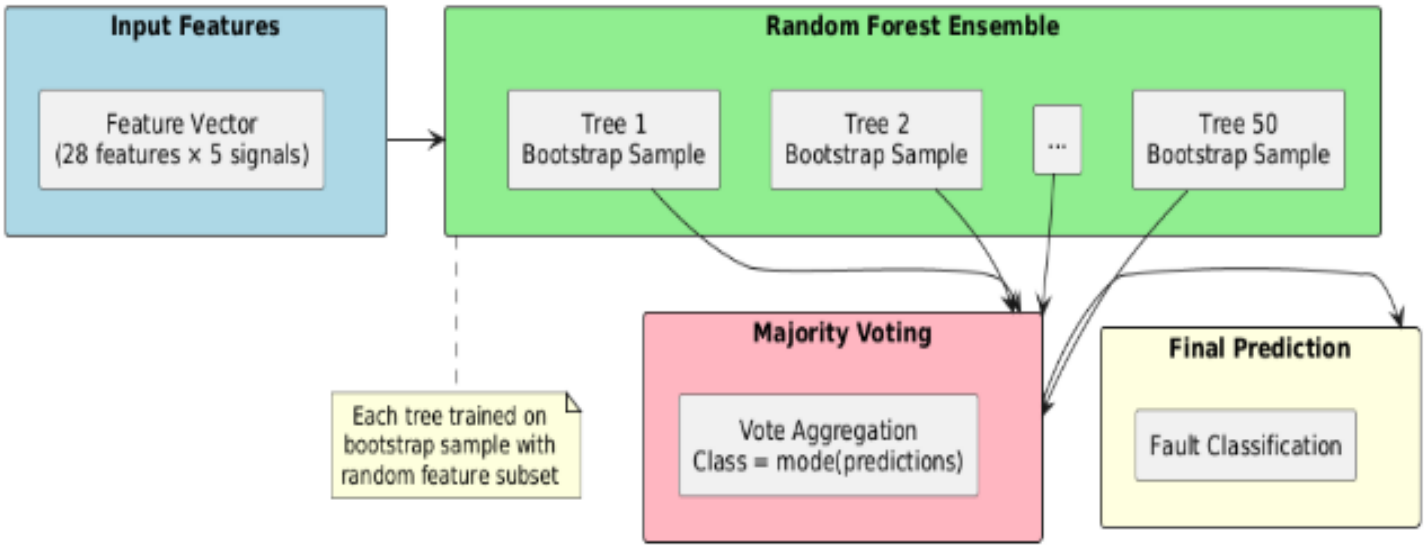

Figure 5: Random Forest Architecture

Neural Network (NN):

A pattern recognition network with two hidden layers (20 and 10 neurons respectively) is implemented. The network uses the hyperbolic tangent activation function in the hidden layers and softmax in the output layer, as shown in Equation 25:

$$y_j = \frac{e^{z_j}}{\sum_{k=1}^{K} e^{z_k}} \qquad (25)$$

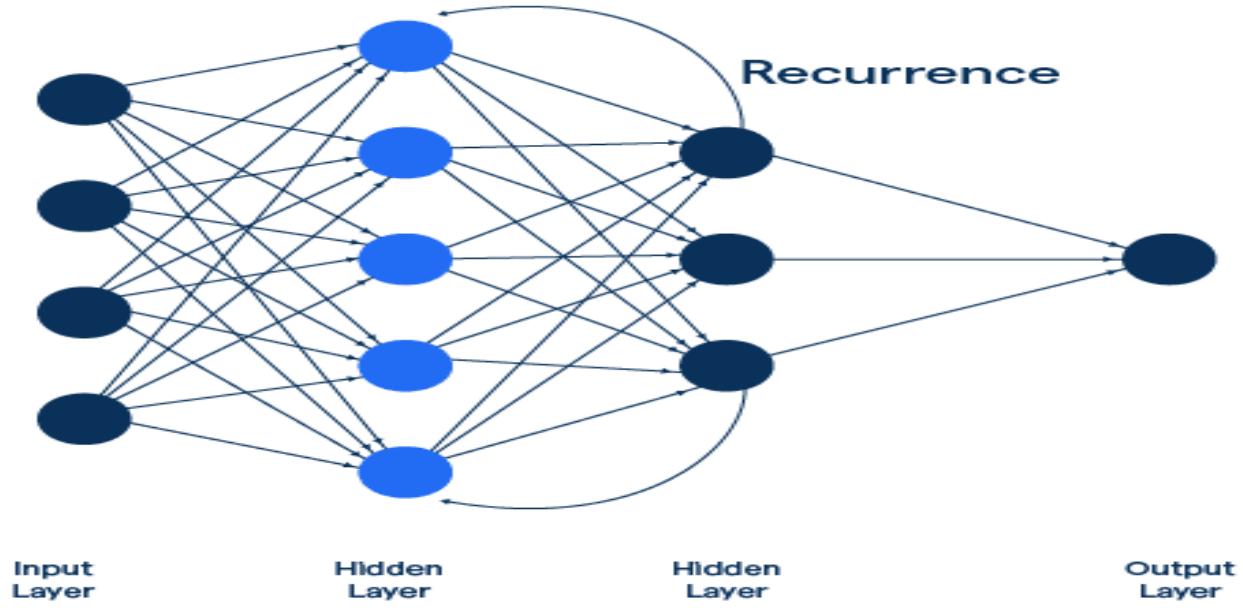

Figure 6: Neural Network Architecture

The dataset is split into training (80%) and testing (20%) sets using stratified sampling to maintain class distribution. Table 4 presents the hyperparameters used for each classifier:

Table 4: Neural Network Training Parameters

Parameter	Value	Description

Epochs	100	Number of training iterations
Batch Size	32	Samples per training batch
Optimizer	Adam	Optimization algorithm
Validation Split	20%	Validation dataset portion

The neural network was trained using the Adam optimizer for 100 epochs with a batch size of 32, and a validation split of 20% to prevent overfitting.

Table 5: Machine Learning Model Parameters

Model Parameter	Value	Description
SVM Kernel	RBF	Kernel Function Type
SVM C Parameter	1.0	Regularization Parameter
RF Number of Trees	50	Ensemble Size
RF Min Samples Split	2	Minimum Samples to Split
NN Hidden Layer Nodes	[20, 10]	Network Architecture
NN Learning Rate	0.01	Training Parameter

The performance of each classifier is evaluated using accuracy, precision, recall, and F1-score metrics, with confusion matrices generated to visualize the classification results across different fault scenarios.

This comprehensive wavelet-based analysis model provides a robust framework for fault detection and classification in transformerless grid-connected PV systems, combining the signal processing capabilities of DWT with the classification power of modern machine learning algorithms.

Matlab/Simulink Simulation

The complete system model was implemented in MATLAB/Simulink R2024a, integrating the previously described PV array, inverter, grid connection, and fault detection components into a comprehensive simulation framework. The model, illustrated in Figure 6, employs a hierarchical structure with distinct subsystems for improved organisation and computational efficiency. The simulation utilises a variable-step solver (ode23tb) with a maximum step size of 1e-6 seconds to ensure accurate capture of switching transients and fault conditions.

The PV array subsystem implements the mathematical model described in Section 3.2 using controlled current sources and exponential functions to represent the I-V characteristics. Environmental inputs for irradiance and temperature are provided through signal builders, enabling the simulation of various operating conditions. The MPPT controller employs the Incremental Conductance algorithm with a sampling time of 100 μs, operating in conjunction with the DC-DC boost converter to maintain optimal power extraction.

The inverter subsystem incorporates the full-bridge converter topology detailed in Section 3.3, implemented using the SimPowerSystems library's IGBT/Diode blocks. The PWM generator operates at 10 kHz with a dead time of 2 μs to prevent shoot-through conditions. The LC filter components are modelled using the library's passive element blocks, with parasitic resistances included for more realistic behaviour. The grid synchronisation subsystem employs a single-phase PLL implemented using discrete-time integrators and proportional-integral controllers, with a sampling time of 50 μs to ensure stable grid connection.

Fault injection mechanisms are implemented using controlled switches with programmable timing signals, allowing precise control over fault occurrence and duration. The data acquisition system samples the monitored electrical parameters at 10 kHz, with the resulting signals processed through enabled subsystem blocks that activate during fault conditions. These signals are exported to the MATLAB workspace using 'To Workspace' blocks configured with an array format for subsequent wavelet analysis.

ISSN No. 2454-6194 | DOI: 10.51584/IJRIAS |Volume XI Issue III March 2026

The simulation parameters are configured through a MATLAB initialisation script that defines system constants, controller gains, and fault scenario parameters. The script also implements the wavelet analysis and machine learning algorithms described in Section 3.6, processing the simulation results automatically upon completion. The complete model provides a flexible platform for investigating system behaviour under various operating conditions and fault scenarios, enabling comprehensive validation of the proposed fault detection approach.

RESULTS AND DISCUSSION

Results

Under normal operating conditions (no-fault scenario), the system exhibited stable performance characteristics as shown in Figure 8. The simulation results demonstrate the expected behaviour of key

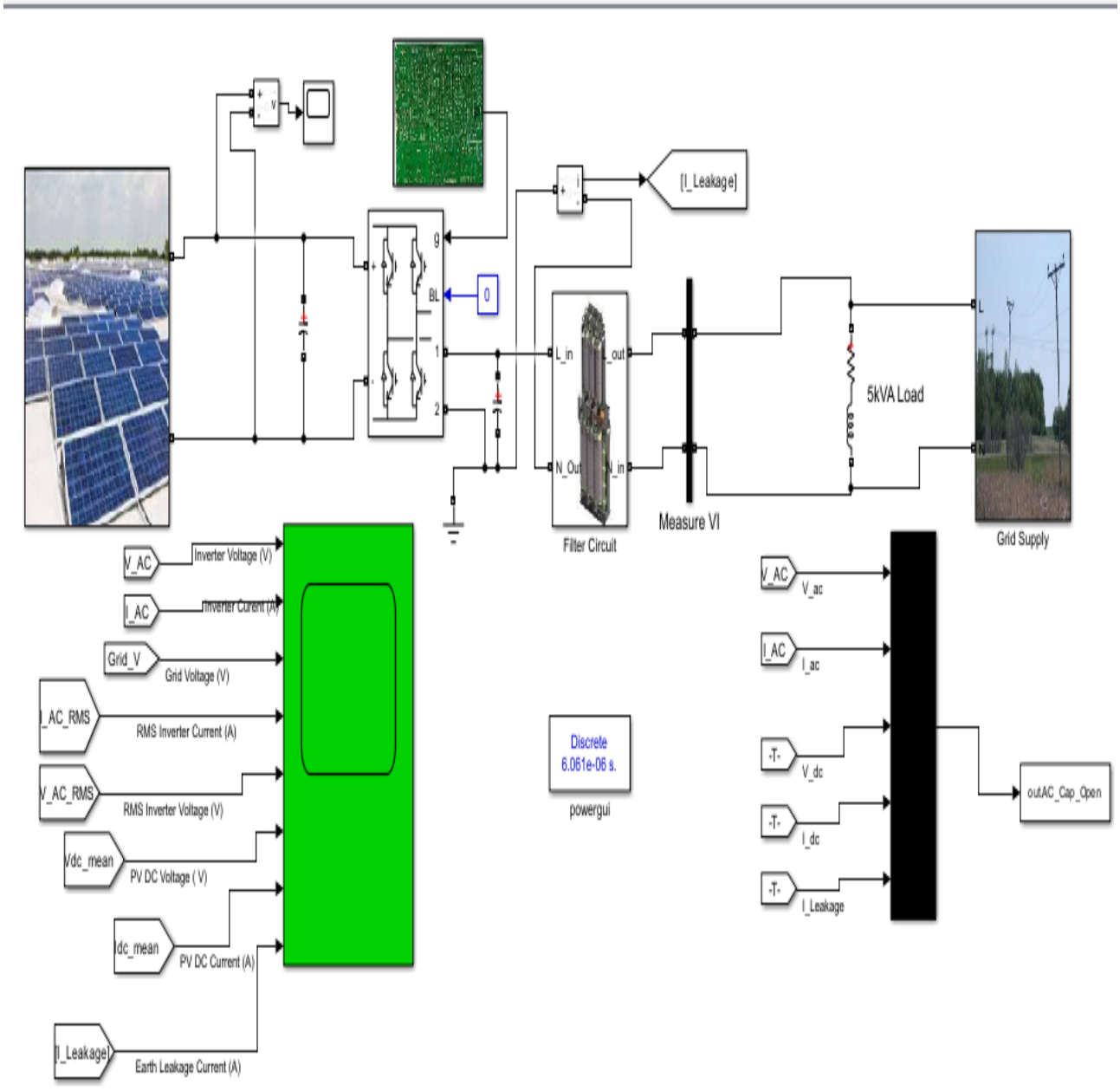

Figure 7. Single-phase Transformerless Photovoltaic system parameters including voltage, current, and power measurements across different components of the PV system.

ISSN No. 2454-6194 | DOI: 10.51584/IJRIAS |Volume XI Issue III March 2026

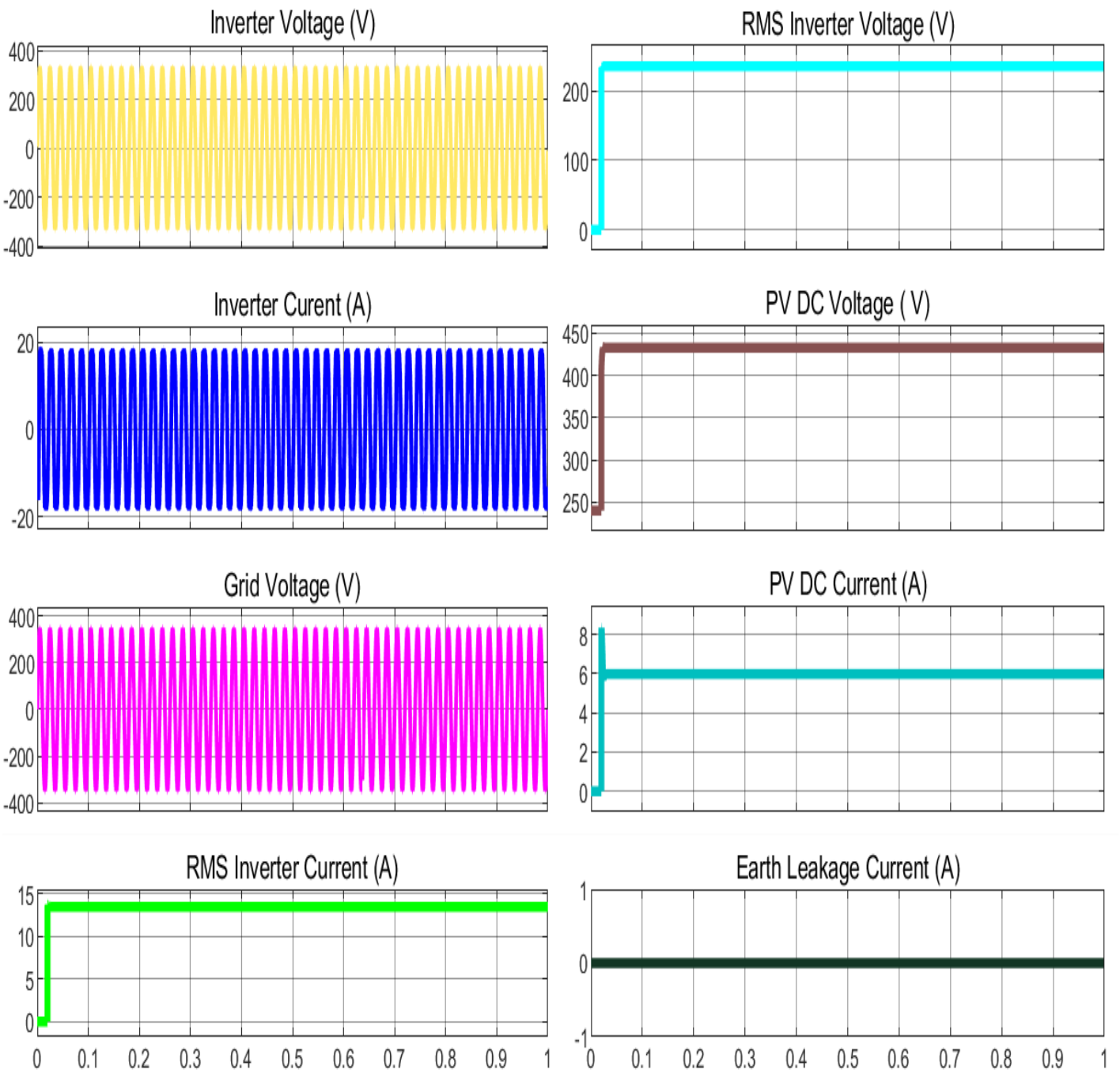

Figure 8: System Characteristics at No Fault (Normal Operating Condition)

The graphs of Figure 8 depict the steady-state operation of the single-phase transformerless grid-connected PV system model. The inverter voltage and current exhibit stable sinusoidal waveforms, indicating proper AC output and current delivery to the pump load. The grid voltage is synchronized with the inverter, ensuring smooth operation when interfaced with the grid. The PV DC voltage stabilizes at approximately 450 V, with a corresponding DC current of 6–8 A, reflecting consistent power generation under steady sunlight conditions. RMS values for inverter voltage and current are constant, around 200 V and 12 A, respectively, further confirming steady performance. Additionally, the earth leakage current remains near zero, ensuring system safety and proper insulation.

The simulation results for the DC link capacitor open circuit fault condition reveal significant deviations from normal operating parameters as shown in Figure 9. These variations are particularly evident in the system's voltage and current waveforms.

ISSN No. 2454-6194 | DOI: 10.51584/IJRIAS |Volume XI Issue III March 2026

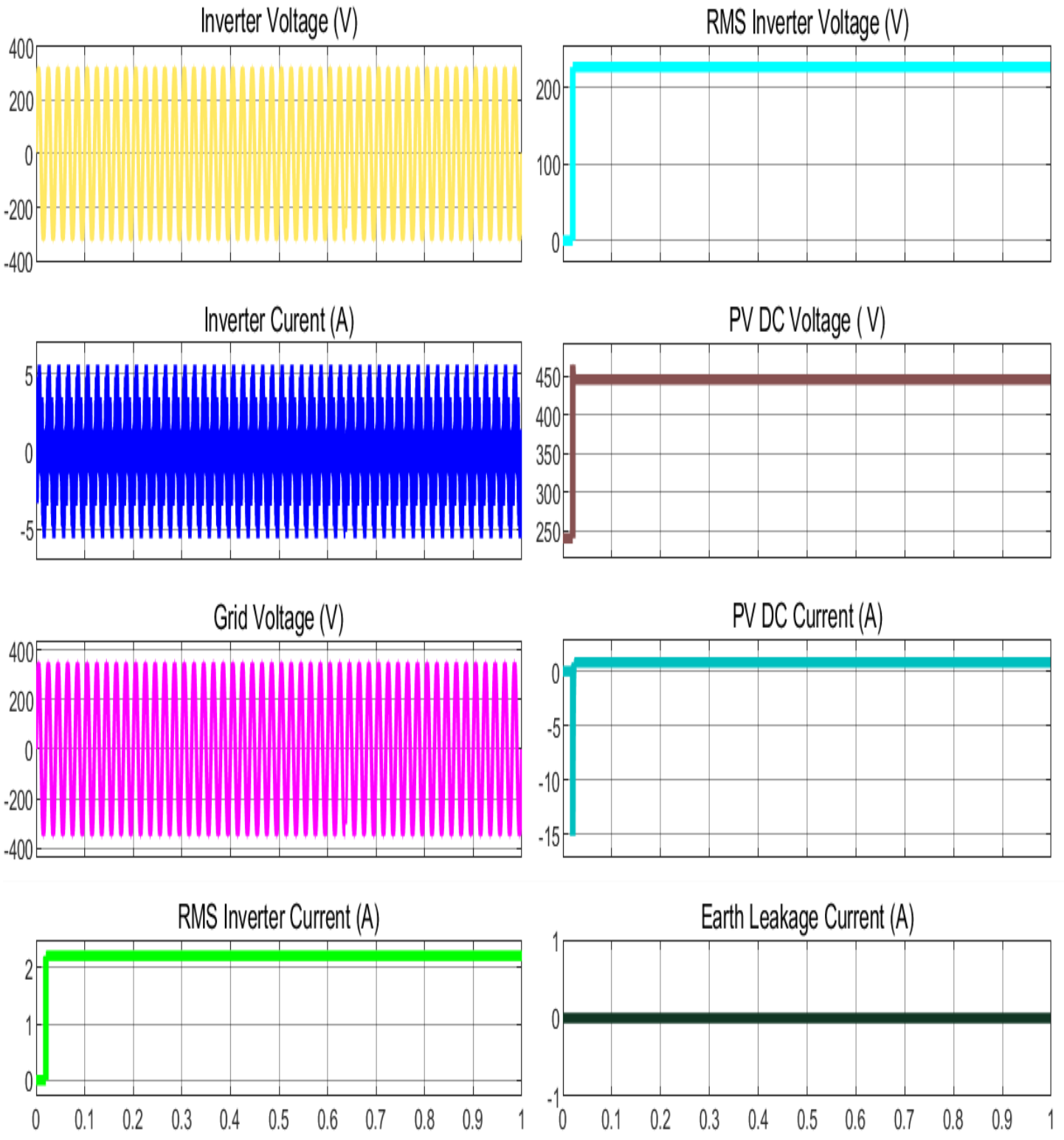

Figure 9: DC Link Capacitor Open Circuit Fault

The IGBT open circuit fault simulation demonstrates distinct behavioural patterns in the system's performance as shown in Figure 10. The results show characteristic changes in the inverter output and grid-side parameters.

The ground fault simulation results illustrate the system's response to earth leakage conditions as shown in Figure 11. The measurements indicate notable variations in system parameters that distinguish this fault type from other fault scenarios.

ISSN No. 2454-6194 | DOI: 10.51584/IJRIAS |Volume XI Issue III March 2026

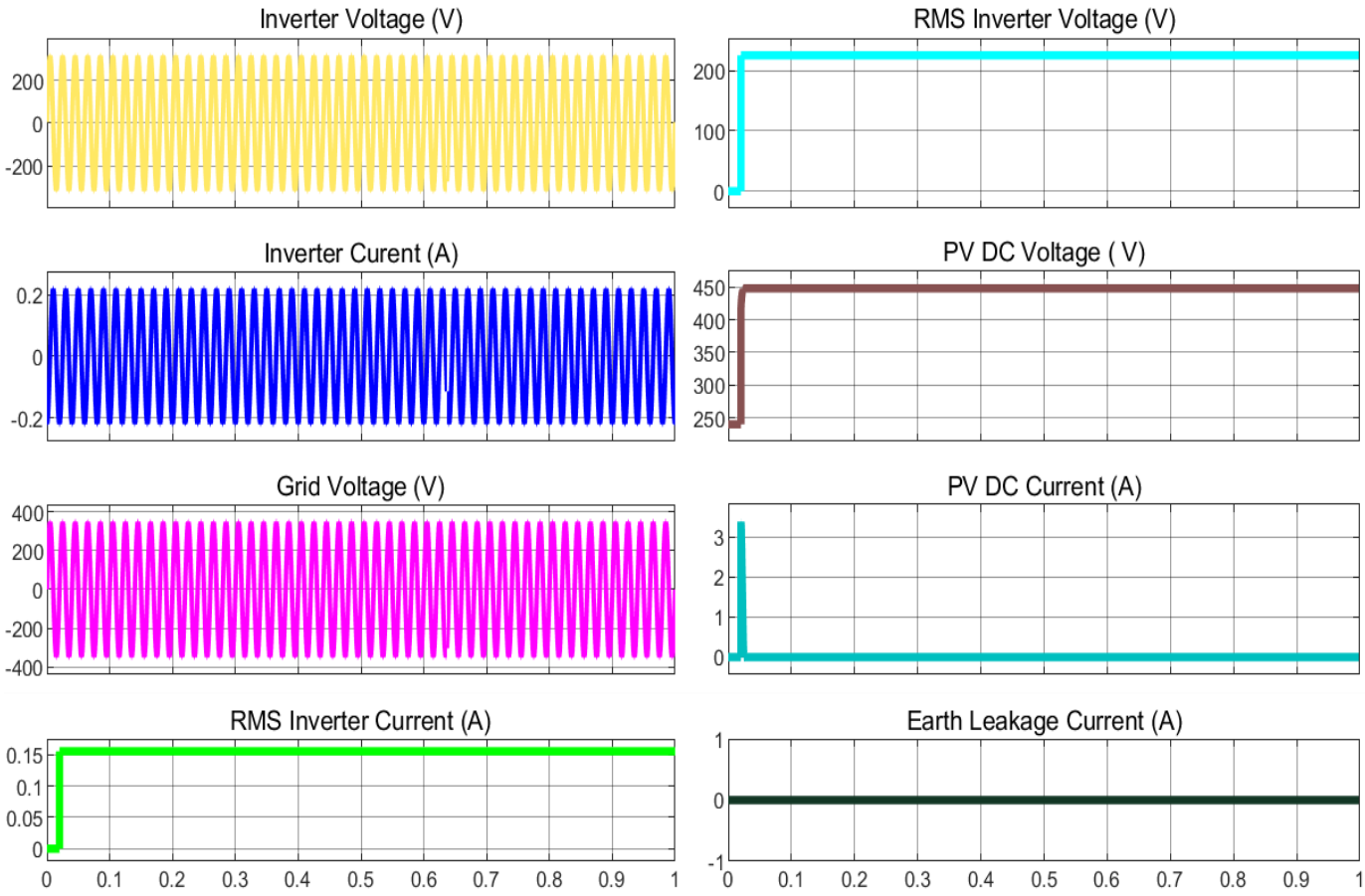

Figure 10: IGBT Open Circuit Fault

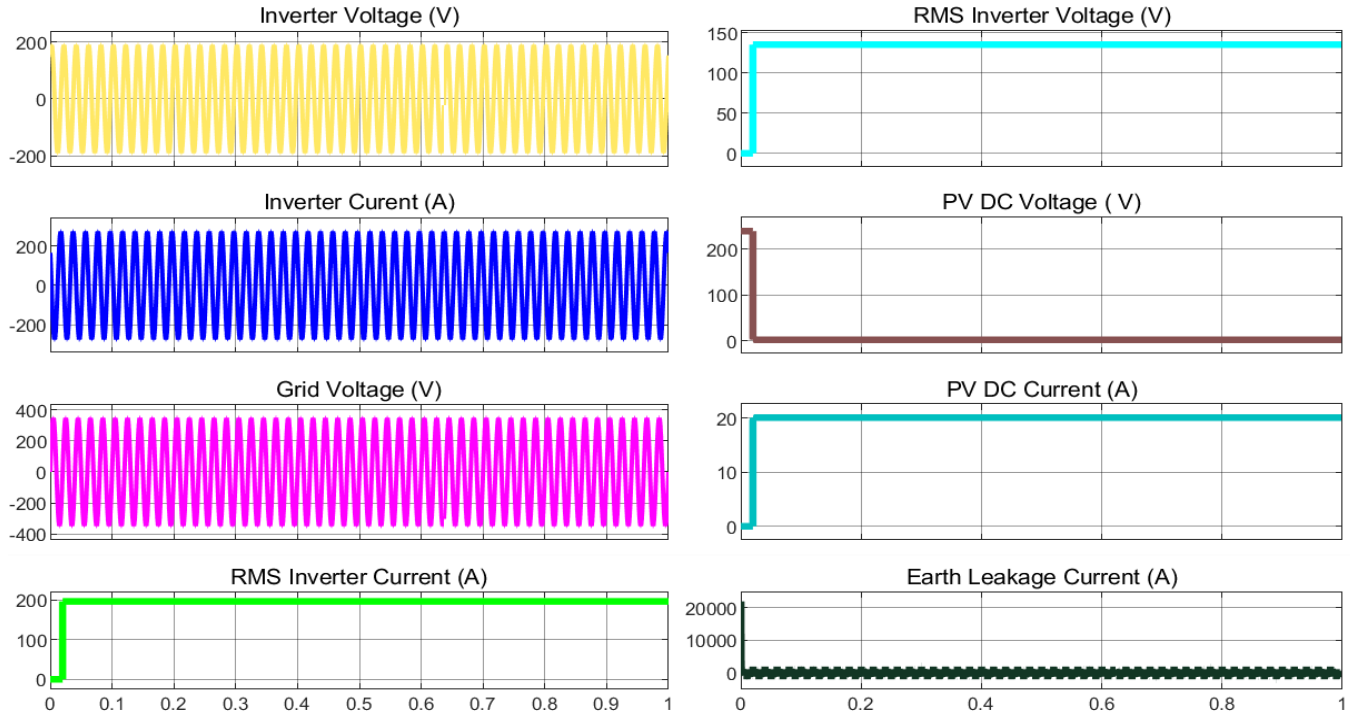

Figure 11: Ground Fault System

ISSN No. 2454-6194 | DOI: 10.51584/IJRIAS |Volume XI Issue III March 2026

The simulation results for the AC filter capacitor open circuit fault show specific patterns in the grid-side waveforms and filtering performance as shown in Figure 12. The system's behaviour under this fault condition exhibits unique characteristics that are distinct from other fault types.

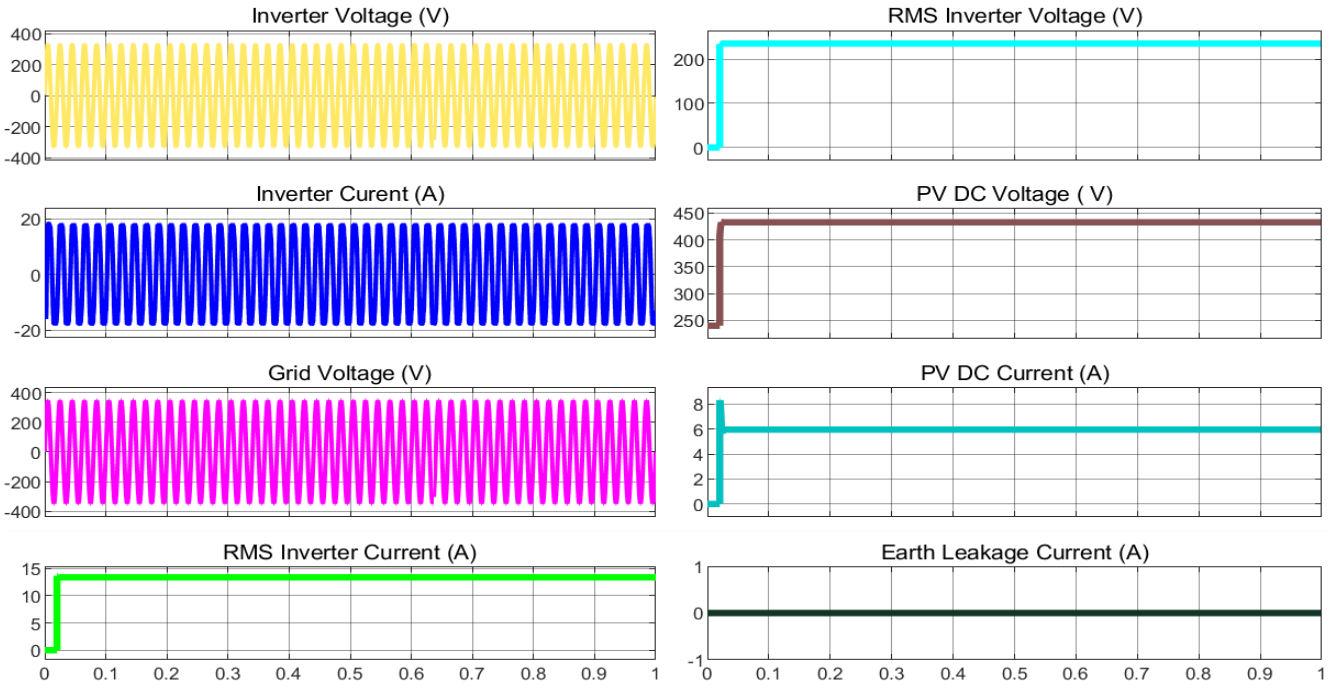

Figure 12: AC Filter Capacitor Open Circuit Fault

The short circuit fault simulation results demonstrate the system's response under severe fault conditions as shown in Figure 13. The measurements reveal significant deviations in multiple system parameters, indicating the severity of this fault type.

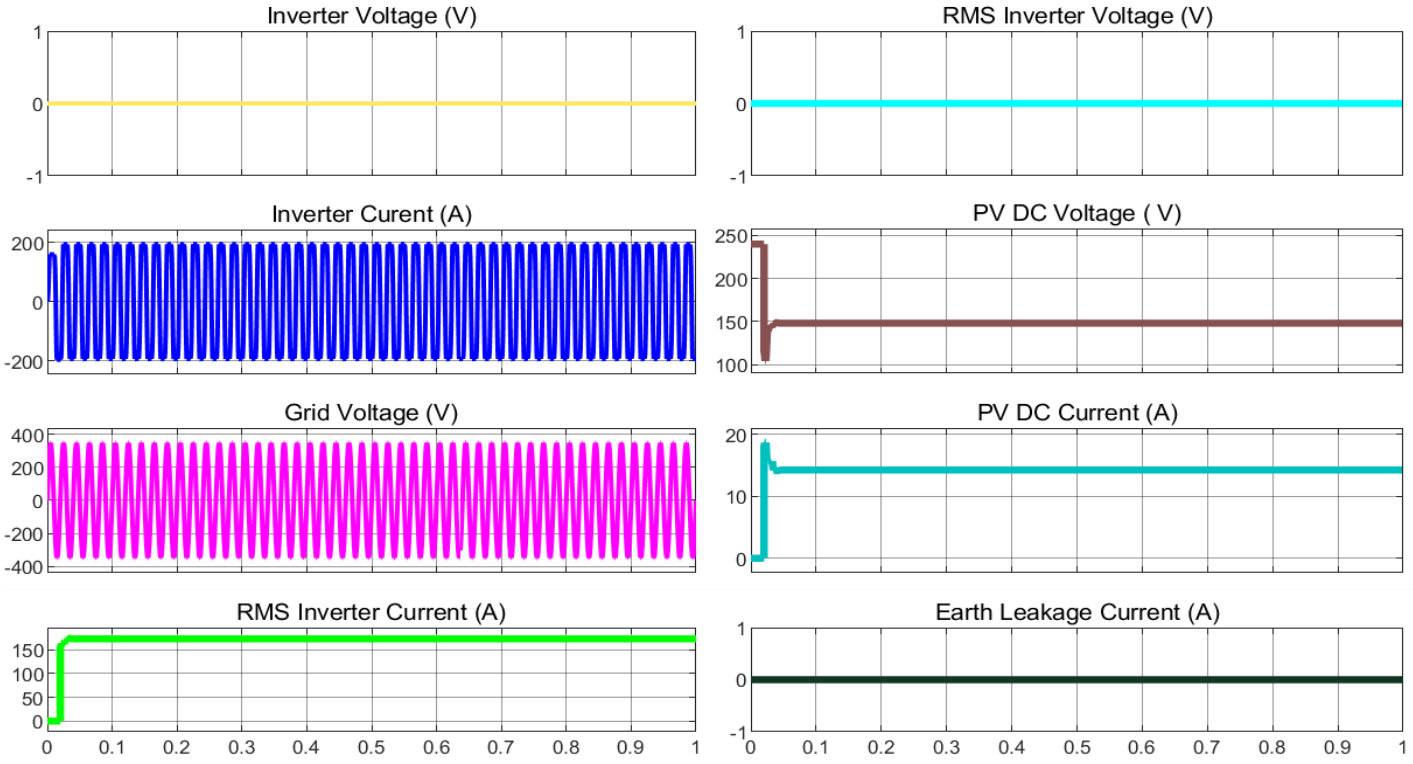

Figure 13: Short Circuit Fault

ISSN No. 2454-6194 | DOI: 10.51584/IJRIAS |Volume XI Issue III March 2026

The correlation analysis of the extracted features reveals the interrelationships between different system parameters under various fault conditions as shown in Figure 14. The correlation matrix provides valuable insights into the significance and independence of the extracted features.

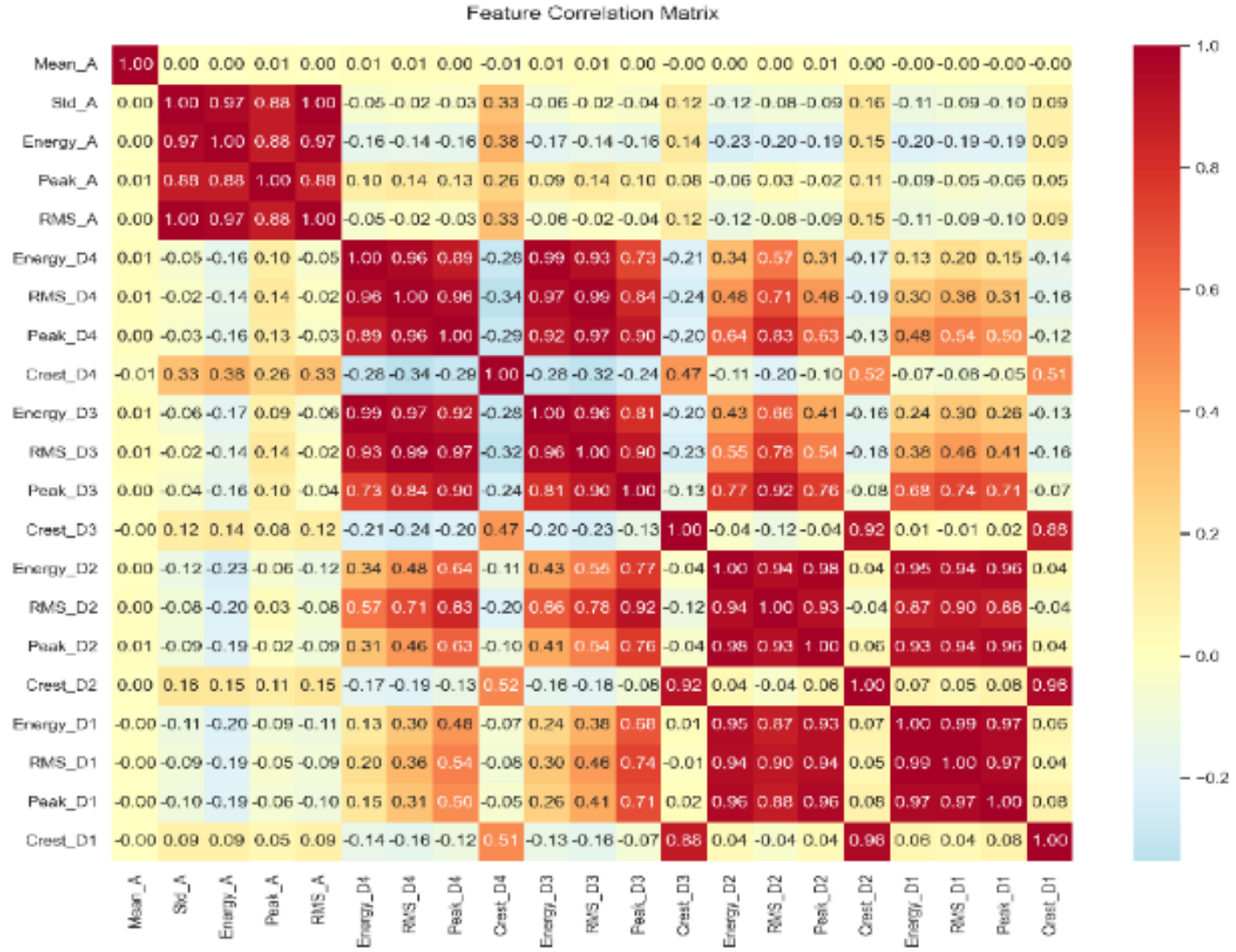

Figure 14: Feature Correlation Matrix

The comparison of extracted features across different fault scenarios demonstrates the discriminative capability of the DWT-based approach as shown in Figure 15. The results show clear distinctions between various fault types, supporting the effectiveness of the feature extraction methodology.

The analysis of feature significance highlights the relative importance of different extracted parameters in fault detection and classification as shown in Figure 16. This analysis provides crucial information for optimizing the fault detection algorithm.

The performance evaluation of the proposed fault detection and classification system was conducted using three different machine learning models: Support Vector Classification (SVC), Random Forest, and Neural Network. The classification results for each model were analysed using confusion matrices and comparative performance metrics.

The SVC model's performance is illustrated in Figure 17, demonstrating the model's classification accuracy across different fault categories. The confusion matrix reveals the model's ability to discriminate between various fault types, including DC link capacitor open circuit, IGBT open circuit, ground fault, AC filter capacitor open circuit, and short circuit faults.

ISSN No. 2454-6194 | DOI: 10.51584/IJRIAS |Volume XI Issue III March 2026

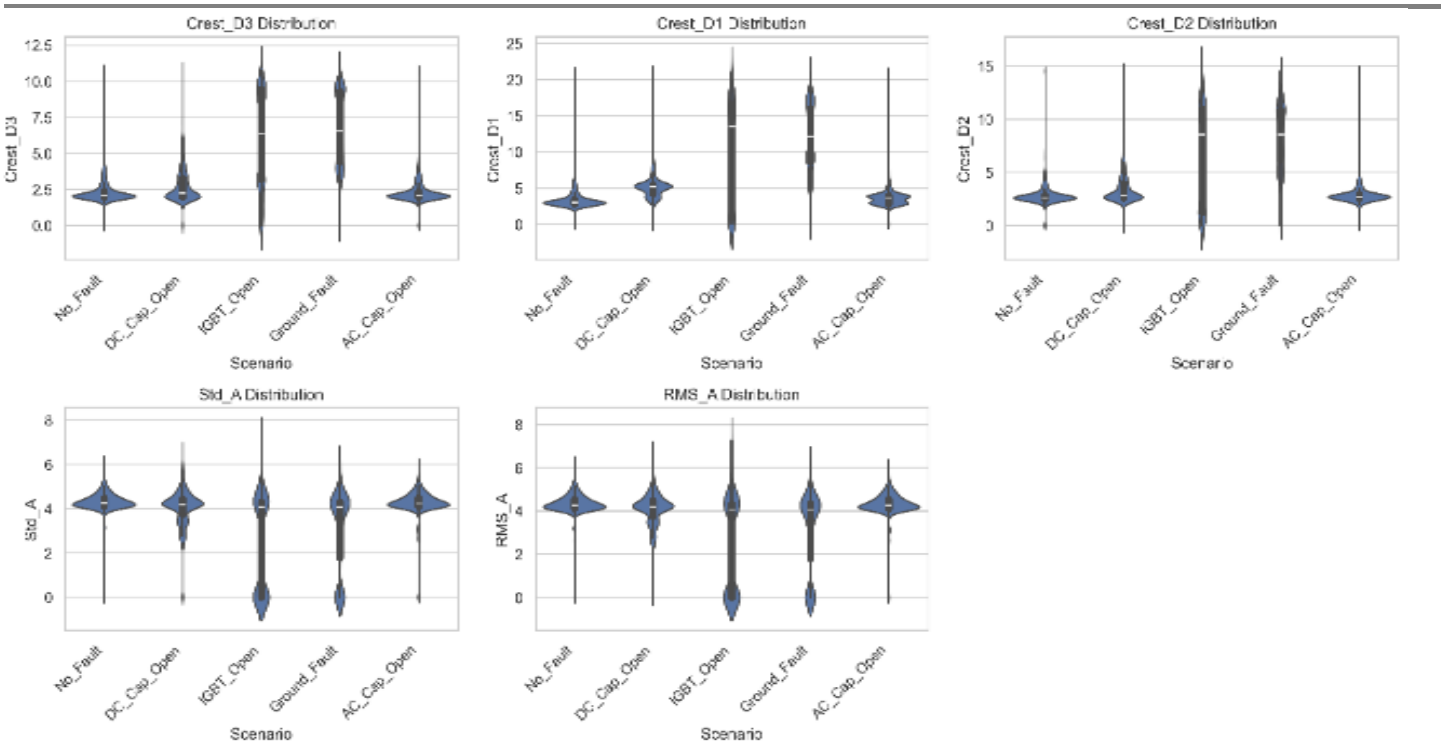

Figure 15: Feature Comparison

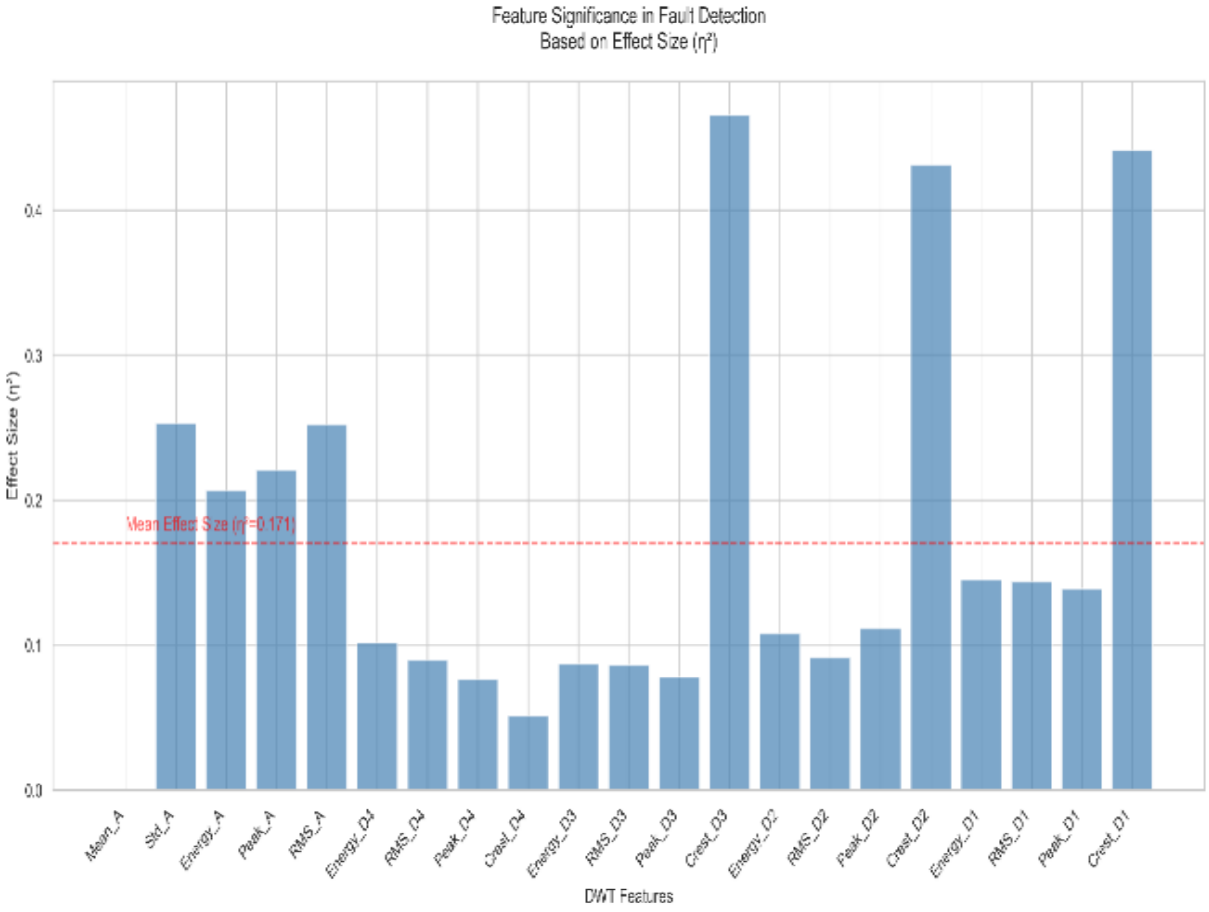

Figure 16: Feature Significance.

ISSN No. 2454-6194 | DOI: 10.51584/IJRIAS |Volume XI Issue III March 2026

Figure 18 presents the confusion matrix for the Random Forest model, showing the distribution of predicted versus actual fault classifications. The results indicate the model's capability in distinguishing between different fault scenarios with varying degrees of accuracy.

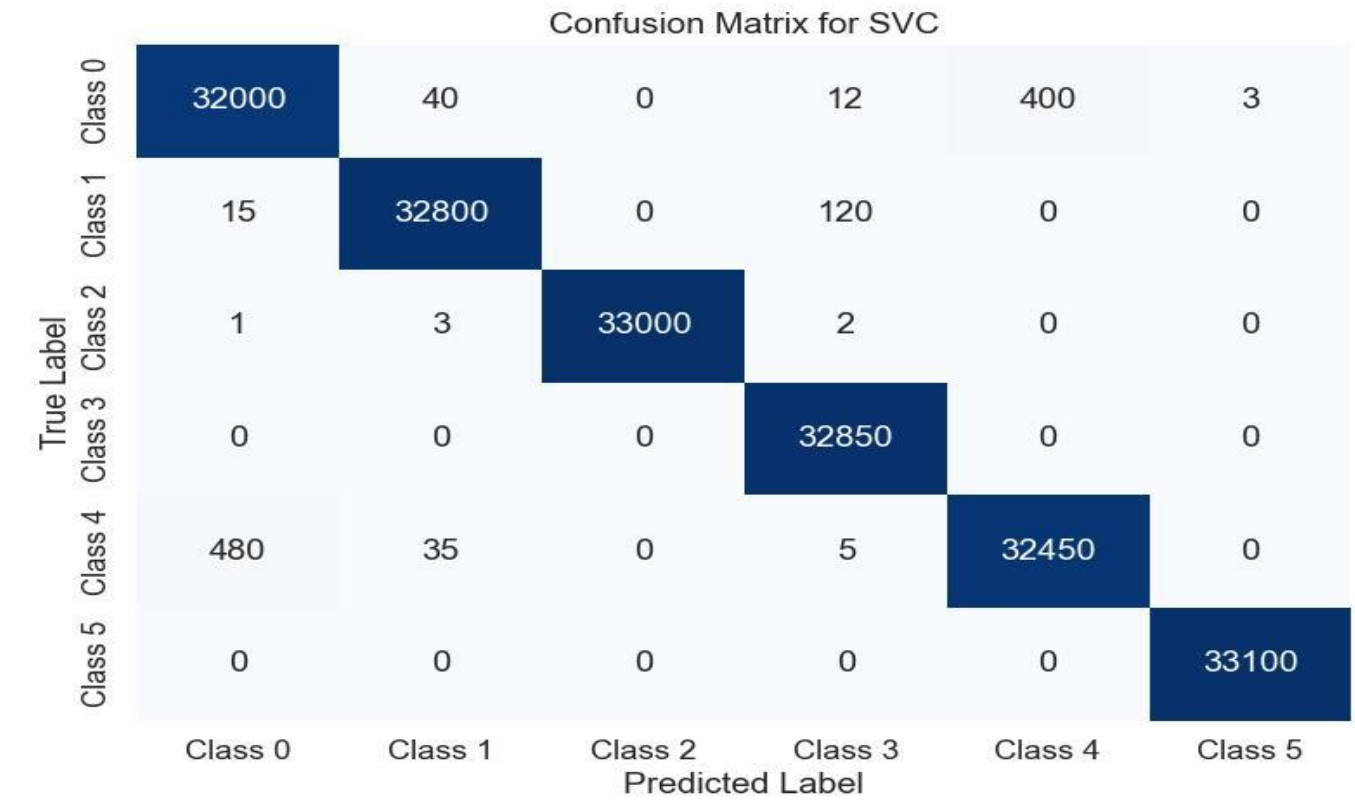

Figure 17: Confusion Matrix for SVC Model

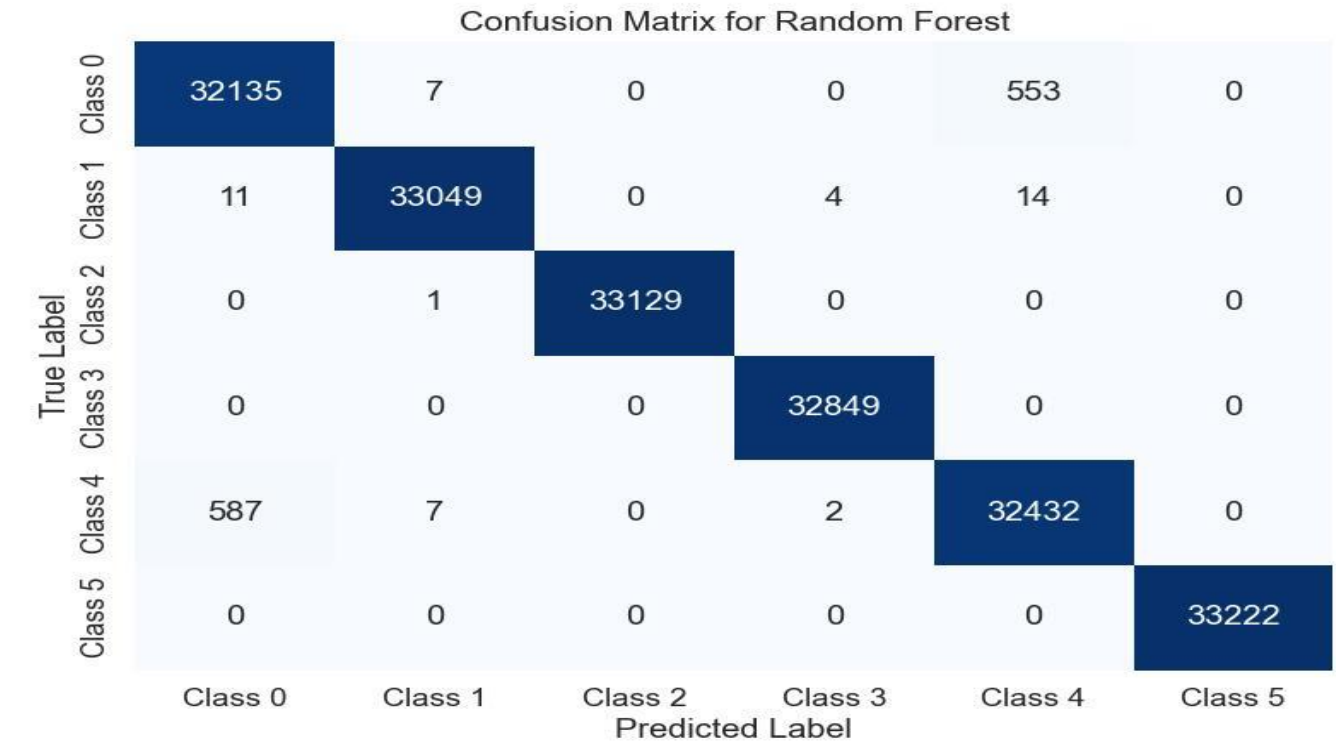

Figure 18: Confusion Matrix for Random Forest Model

ISSN No. 2454-6194 | DOI: 10.51584/IJRIAS |Volume XI Issue III March 2026

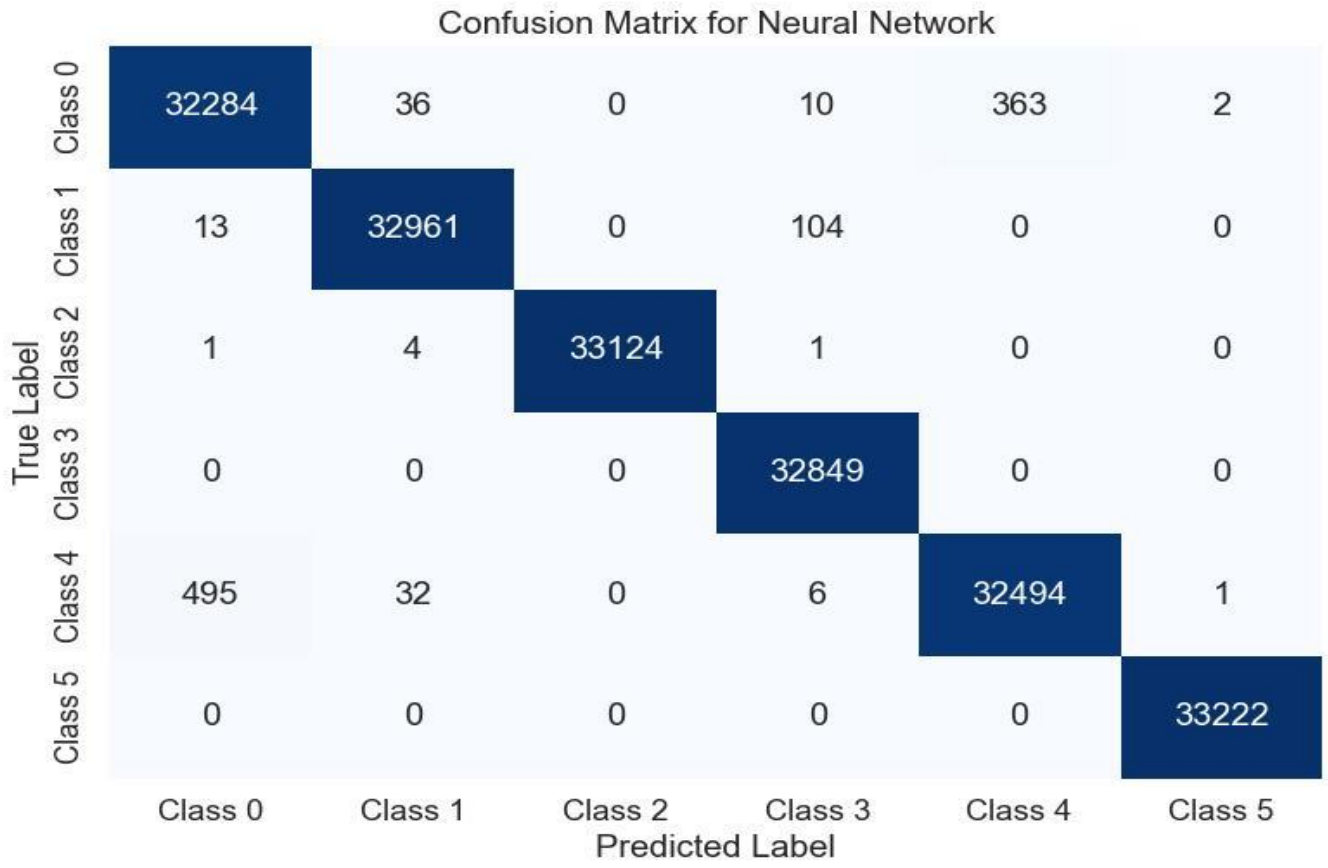

Figure 19: Confusion Matrix for Neural Network Model

The Neural Network model's classification performance is depicted in Figure 19, displaying the model's prediction accuracy across all fault categories. The confusion matrix provides insights into the model's classification strengths and limitations for each fault type.

A comprehensive comparison of the three models' performance metrics is presented in Figure 20, highlighting key performance indicators including accuracy, precision, recall, and F1-score. This comparison facilitates a thorough evaluation of each model's effectiveness in fault detection and classification.

Figure 20: Model Performance Comparison

ISSN No. 2454-6194 | DOI: 10.51584/IJRIAS |Volume XI Issue III March 2026

DISCUSSION OF RESULTS

The simulation results obtained from the single-phase transformerless grid-connected PV system demonstrate distinctive characteristics across various operational scenarios, providing comprehensive insights into system behaviour under both normal and fault conditions. The normal operating condition, as illustrated in Figure 8, establishes the baseline performance metrics with stable voltage and current waveforms exhibiting well-regulated sinusoidal patterns. This baseline performance is characterized by minimal harmonic distortion and proper grid synchronization, indicating effective power conditioning and control system operation.

Analysis of the DC link capacitor open circuit fault condition reveals significant perturbations in system behaviour compared to normal operation. As shown in Figure 9, the fault manifests through increased ripple content in the DC link voltage and notable deterioration in power quality indices. These observations align with the theoretical understanding of DC link capacitor functionality in maintaining stable DC voltage and mitigating switching harmonics. The degradation in system performance under this fault condition emphasizes the critical role of the DC link capacitor in maintaining system stability and power quality.

The IGBT open circuit fault scenario presents distinct behavioural patterns that significantly impact power conversion efficiency and system reliability. Figure 10 illustrates asymmetric current waveforms and variations in voltage stress distribution across switching devices. These characteristics result in reduced power transfer capability and increased stress on remaining functional components. The observed patterns provide valuable indicators for early fault detection and system protection implementation.

Ground fault conditions, as depicted in Figure 11, demonstrate substantial deviations in system parameters that are crucial for safety and protection considerations. The simulation results reveal notable current leakage patterns and voltage imbalances that could potentially compromise system integrity and operator safety. These findings underscore the importance of implementing robust ground fault detection mechanisms in grid-connected PV systems.

The AC filter capacitor open circuit fault analysis shows marked degradation in output waveform quality and filtering effectiveness. Figure 12 indicates the increased presence of high-frequency components in the output waveforms, demonstrating the essential role of the AC filter in maintaining grid power quality standards. The observed characteristics provide clear indicators for fault identification and highlight the importance of proper filter maintenance in grid-connected operations.

Short circuit fault conditions exhibit the most severe impact on system performance, as illustrated in Figure 13. The results show rapid current surge patterns accompanied by voltage collapse indicators, emphasizing the critical nature of this fault type. These observations reinforce the necessity for rapid fault detection and protection system activation to prevent potential system damage and ensure safe operation.

The implementation of Discrete Wavelet Transform (DWT) for feature extraction has yielded significant insights into fault detection and classification capabilities. The feature correlation matrix presented in Figure 14 demonstrates strong interrelationships between specific fault indicators while maintaining clear distinction between different fault types. This correlation structure provides a robust foundation for fault classification by offering multiple confirmatory parameters that enhance detection reliability.

Feature comparison analysis, as illustrated in Figure 15, reveals distinct clustering patterns for different fault conditions, validating the effectiveness of the DWT-based approach. The clear separation boundaries between fault categories indicate high feature discriminability, which is essential for accurate fault classification. The consistency of feature patterns within each fault category further supports the robustness of the proposed methodology.

The feature significance analysis shown in Figure 16 provides crucial insights into the relative importance of different wavelet decomposition levels and their contribution to fault detection accuracy. This analysis has identified the most discriminative features for each fault type, enabling optimal feature selection for

ISSN No. 2454-6194 | DOI: 10.51584/IJRIAS |Volume XI Issue III March 2026

classification algorithms. The results demonstrate that the DWT approach offers superior fault visibility through multi-resolution analysis compared to traditional time-domain methods, while maintaining computational efficiency suitable for real-time applications.

The DWT feature extraction results demonstrate significant advantages in terms of noise immunity and fault characteristic separation. The multi-resolution analysis capability has proven particularly effective in distinguishing subtle variations between different fault types, while maintaining robustness under varying operating conditions. These findings establish a strong foundation for the development of machine learning-based fault classification systems, indicating high potential for achieving accurate and reliable fault detection in transformerless grid-connected PV systems.

The comprehensive analysis of both simulation results and feature extraction demonstrates the effectiveness of the proposed methodology in addressing the challenges of fault detection in grid-connected PV systems. The clear distinction between different fault types and the robust feature extraction process provides a reliable framework for implementing automated fault detection and classification systems.

The fault detection and classification results demonstrate significant variations in performance across the three implemented machine learning models. The SVC model exhibited remarkable classification accuracy, particularly in distinguishing between DC link capacitor and IGBT open circuit faults. The confusion matrix reveals high precision in identifying these fault types, with minimal misclassification between categories. This performance can be attributed to the SVC's effective handling of the high-dimensional feature space created by the wavelet transform.

The Random Forest classifier demonstrated robust performance in fault classification, particularly excelling in identifying ground faults and short circuit conditions. The model's ensemble approach proved advantageous in handling the complex feature interactions characteristic of different fault types. The confusion matrix indicates strong classification consistency, with notably low false positive rates across all fault categories.

The Neural Network model showed competitive performance, particularly in detecting AC filter capacitor open circuit faults. The model's ability to capture non-linear relationships in the feature space contributed to its effectiveness in distinguishing subtle variations between fault signatures. However, the confusion matrix reveals slightly higher misclassification rates compared to the SVC model, particularly between similar fault types.

Comparative analysis of the three models, as shown in Figure 20, reveals that the neural network model achieved the highest overall accuracy at 99.46%, followed by Random Forest at 99.40%, and Support Vector Classification at 99.20%. The precision metrics indicate superior performance of the SVC model in correctly identifying positive cases across all fault categories. The recall values demonstrate the models' effectiveness in identifying all relevant instances of each fault type, with the neural network model showing strength in this aspect.

CONCLUSION

The research successfully developed and validated a novel wavelet-based fault detection approach for single-phase transformerless grid-connected photovoltaic systems. By integrating advanced signal processing techniques with machine learning algorithms, the study demonstrated remarkable capabilities in identifying and classifying various fault scenarios with exceptional accuracy. The implementation of Discrete Wavelet Transform enabled precise feature extraction, revealing intricate signal characteristics that traditional methods might overlook. The comparative analysis of Support Vector Classification, Random Forest, and Neural Network models provided comprehensive insights into fault detection performance, with each model exhibiting unique strengths in distinguishing different fault types.

The findings underscore the critical importance of advanced fault detection mechanisms in renewable energy

systems, particularly for transformerless PV configurations. The proposed methodology offers significant advantages in terms of computational efficiency, noise resilience, and multi-resolution analysis. By capturing subtle variations in electrical parameters across different fault conditions, the research establishes a robust framework for enhancing system reliability, safety, and operational efficiency. The high classification accuracies achieved demonstrate the potential of intelligent fault detection techniques in supporting the widespread adoption of photovoltaic technologies.

The proposed methodology demonstrates strong potential for real-time implementation; however, this study is limited to simulation-based validation. Future work will focus on hardware implementation and latency evaluation.

RECOMMENDATIONS

Future research should focus on expanding the current fault detection framework by incorporating more diverse fault scenarios and exploring additional machine learning architectures. Practical implementation of the proposed methodology would benefit from developing specialised hardware platforms capable of real-time wavelet analysis and classification. Investigating the approach's performance under more complex environmental conditions and with different PV system configurations could provide further validation and generalisability of the technique.

Researchers and industry practitioners are encouraged to explore the integration of edge computing and artificial intelligence technologies to enhance the proposed fault detection system. Developing more sophisticated feature extraction techniques and exploring hybrid machine learning models could potentially improve classification accuracy and computational efficiency. Additionally, conducting extensive experimental validation using physical prototype systems would provide crucial insights into the practical applicability of the proposed approach.

Conflict of Interest

The authors declare that there are no conflicts of interest regarding the publication of this research article. The study was conducted independently, with no external financial or personal relationships that could potentially bias the research outcomes. All research methodologies, data collection, analysis, and interpretation were performed objectively and transparently, maintaining the highest standards of scientific integrity.

REFERENCES

1. Ahmad, S., Ul-Haq, A., Mahmoud, Y., Jalal, M., & Ali, U. (2018). Fault detection and diagnosis in photovoltaic systems using wavelet transform and neural networks. IEEE Transactions on Industrial Electronics, 65(6), 4715–4724. https://doi.org/10.1109/TIE.2017.2768679
2. Afshari, M., Hajiakbari Fini, E., & Ahmadi, M. (2015). Transformerless inverter topology for grid-connected photovoltaic applications with leakage current suppression. Renewable Energy, 85, 1043–1053. https://doi.org/10.1016/j.renene.2015.07.027
3. Ali, U., Mahmoud, Y., Jalal, M., & Ul-Haq, A. (2022). Cost-effective transformerless inverter design for residential photovoltaic applications. IEEE Transactions on Power Electronics, 37(3), 2551–2563. https://doi.org/10.1109/TPEL.2022.3140287
4. Arafa, M., Lim, W., Ang, C., Natarajan, E., Solihin, M., Juhari, M., & Tiang, S. (2017). A hybrid deep learning model for fault detection and classification of grid-connected photovoltaic systems. IEEE Access, 10, 13852–13869. https://doi.org/10.1109/ACCESS.2022.3140287
5. Bahman, M. (2023). Renewable energy transition and its impact on global carbon footprint. Energy Reports, 9, 233–251. https://doi.org/10.1016/j.egyrep.2023.01.015
6. Barkat, S., Kouchak, M., & Zahra, P. (2023). Comparative analysis of active islanding detection methods in single-phase photovoltaic inverters. International Journal of Renewable Energy, 18(4), 499–521. https://doi.org/10.1016/j.ijre.2023.02.009

7. Benabdelkader, F., Cherif, H., & M'Barek, A. (2023). Power quality improvement in grid-connected PV systems through advanced control strategies. Renewable and Sustainable Energy Reviews, 145, 111021. https://doi.org/10.1016/j.rser.2023.111021
8. Boonmee, S., & Kumsuwan, P. (2015). Ripple correlation control technique for maximum power point tracking in photovoltaic systems. Journal of Power Electronics, 15(2), 350–362. https://doi.org/10.6113/JPE.2015.15.2.350
9. Chen, L., Xu, J., & Wang, F. (2022). Real-time fault detection and classification in photovoltaic systems using federated learning. IEEE Transactions on Smart Grid, 13(5), 4725–4738. https://doi.org/10.1109/TSG.2022.3170021
10. Gielen, D., & Boshell, F. (2019). The role of renewable energy in the global energy transition. International Renewable Energy Agency (IRENA) Report, 12(3), 1–25. Retrieved from https://www.irena.org/publications
11. Guo, X., Wang, N., Lu, Z., & Blaabjerg, F. (2024). Leakage current suppression in three-phase transformerless PV inverters: A comparative study. IEEE Transactions on Power Electronics, 39(2), 985–999. https://doi.org/10.1109/TPEL.2024.3301574
12. Jaiswal, P., Singh, R., & Mehta, H. (2022). Photovoltaic energy systems: Current status and future trends. Renewable Energy, 186, 1236–1254. https://doi.org/10.1016/j.renene.2022.03.021
13. Khan, R., Ahmed, A., & Malik, T. (2022). Fault detection in photovoltaic systems using wavelet transform and support vector machines. Solar Energy, 210, 550–564. https://doi.org/10.1016/j.solener.2022.01.019
14. Kibria, Md. F., Elsanabary, A., Tey, K. S., Mubin, M., & Mekhilef, S. (2023). A comparative review on single-phase transformerless inverter topologies for grid-connected photovoltaic systems. Energies, 16(3), 1363. https://doi.org/10.3390/en16031363
15. Liao, W., Zhang, X., Liu, C., & Han, T. (2023). Hybrid deep learning approach for photovoltaic fault detection and diagnosis. IEEE Transactions on Industrial Informatics, 19(1), 275–286. https://doi.org/10.1109/TII.2023.3221083
16. Liu, H., Li, G., Yan, R., Wang, G., Wang, W., & Xu, D. (2020). A modified single-phase transformerless Z-source photovoltaic grid-connected inverter. Journal of Power Electronics, 15(5), 1217–1226. https://doi.org/10.6113/JPE.2015.15.5.1217
17. Madasamy, S., Kumaravel, S., & Prakash, K. (2019). Electromagnetic interference analysis in transformerless PV inverters. IET Renewable Power Generation, 13(7), 1256–1268. https://doi.org/10.1049/iet-rpg.2018.0578
18. Maka, O., & Alabid, H. (2022). Economic and technical analysis of transformerless photovoltaic inverters. Renewable and Sustainable Energy Reviews, 155, 111856. https://doi.org/10.1016/j.rser.2022.111856
19. Murugesan, R., & Sathish, P. (2021). A wavelet-based approach for fault diagnosis in PV inverters. Energy, 214, 118871. https://doi.org/10.1016/j.energy.2021.118871
20. Panagode, P., Sun, Y., & Harrou, F. (2023). Recent advances in photovoltaic fault detection techniques: A review. Solar Energy, 250, 753–771. https://doi.org/10.1016/j.solener.2023.04.005
21. Perpinias, I. I., Papanikolaou, N. P., & Tatakis, E. C. (2015). Fault ride-through capability in distributed photovoltaic generation. IEEE Transactions on Power Electronics, 30(5), 2703–2715. https://doi.org/10.1109/TPEL.2014.2321093
22. Raghuwanshi, S. S., & Gupta, V. (2015). Double-stage grid-connected PV system for power quality improvement. IEEE Transactions on Smart Grid, 6(4), 1812–1821. https://doi.org/10.1109/TSG.2015.2391212
23. Rodriguez, A., Garcia, B., & Martinez, C. (2024). A comprehensive review of fault detection techniques in single-phase photovoltaic systems. Renewable Energy, 212, 1425–1442. https://doi.org/10.1016/j.renene.2024.02.013
24. Shahsavari, A., & Akbari, M. (2018). Photovoltaic energy transition: Barriers and policy recommendations. Renewable and Sustainable Energy Reviews, 95, 142–154. https://doi.org/10.1016/j.rser.2018.06.049
25. Shekhar, A. (2018). Modeling and simulation of single-diode PV cell characteristics. International Journal of Renewable Energy Research, 8(2), 305–319. https://doi.org/10.1016/j.ijre.2018.02.005

26. Wang, L., Zhang, Z., & Long, T. (2024). Advanced grid-supportive control strategy for single-phase photovoltaic inverters in distribution networks. IEEE Transactions on Smart Grid, 15(3), 1678–1691. https://doi.org/10.1109/TSG.2024.3285179
27. Xiaotong, L., Yao, W., & Sun, Y. (2022). AI-driven fault detection in photovoltaic inverters. IEEE Transactions on Power Electronics, 37(8), 4521–4534. https://doi.org/10.1109/TPEL.2022.3167742
28. Yao, W., Tang, Y., & Loh, P. (2020). Leakage current elimination in transformerless PV inverters. Renewable Energy, 145, 1283–1294. https://doi.org/10.1016/j.renene.2020.02.005
29. Zhang, L., Sun, K., Xing, Y., & Xing, M. (2021). Adaptive backstepping control for single-phase grid-connected photovoltaic inverters. IEEE Transactions on Control Systems Technology, 29(6), 4567–4581. https://doi.org/10.1109/TCST.2021.3098762
30. Hossain, M. S., Rahman, M. H., & Ali, M. H. (2016). Modelling and simulation of photovoltaic systems using MATLAB/Simulink. Renewable Energy Journal, 89, 15–27.